

12 Pumped Fluid Loops

T. T. Lam,* G. C. Birur,† and P. Bhandari†

Introduction

Spacecraft thermal control techniques can be categorized as passive thermal control (PTC) or active thermal control (ATC). PTC can be achieved by control of conductive and radiative heat paths through selection of the proper geometrical configurations, insulation blankets, sun shields, radiating fins, surface thermo-optical properties, thermal coatings, heat sinks, and phase-change materials. A PTC system does not involve moving parts or fluids. The spacecraft component temperatures are maintained within the desired range by proper control of the dissipated energy between all spacecraft elements through the conductive and radiative heat paths. However, to execute a design in which the PTC techniques cannot deal with environmental extremes or to accommodate equipment dissipating high power, employment of ATC techniques may be more efficient. In such cases, designs can be executed by the use of heaters, louvers, heat pipes, thermoelectric coolers, cryogenic coolers, and pumped fluid loops (PFLs).

PFLs are devices that provide efficient transfer of a large amount of thermal energy between two points by means of forced liquid convective cooling. PFLs for space applications are the subject of this chapter. A simplified PFL, as shown in Fig. 12.1, consists of a pumping device, a heat exchanger, and a space radiator. The cooling can be accomplished by the use of a coolant as the thermal energy transport agent. The coolant absorbs the dissipated thermal energy from a component and transfers it to a heat sink. The final heat-rejection process depends on whether the coolant is expendable or nonexpendable. With expendable coolant,

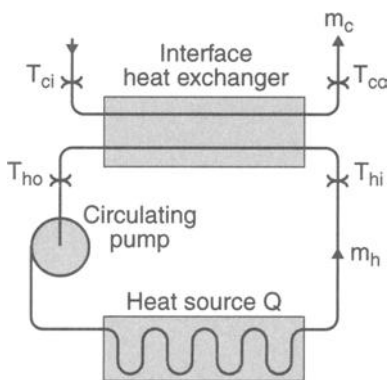


Fig. 12.1. Schematic of a simplified PFL system.

*The Aerospace Corporation, El Segundo, California.

†Jet Propulsion Laboratory, California Institute of Technology, Pasadena, California.

the working fluid is rejected from the space vehicle once it has accomplished its mission. In the case of nonexpendable coolant, the working fluid is recirculated within the system once its thermal energy has been radiated to space via a radiator.

Space vehicles of recent years, such as the Defense Satellite Program and the space shuttle orbiter, have used PFLs in their ATC subsystems. The schematic orbiter ATC subsystem is depicted in Fig. 12.2. The subsystem collects excess heat from the cabin interchanger, the fuel-cell heat exchanger, the hydraulics heat exchanger, the GSE (ground support equipment) heat exchanger, and the payload heat exchanger, and it ejects heat from the orbiter to space. The ATC payload-cooling elements consist of the radiator panels, the flash evaporator, the aft cold plates, and the ammonia boiler. The radiators provide cooling for the payload while the payload-bay doors are open on orbit. As the flow diagram suggests, the thermal control design of an ATC subsystem with PFLs is normally more difficult than that of a PTC subsystem. Subsequent sections of this chapter explain the PFL design in detail.

In what follows, basic fluid-flow equations and friction analysis of pipes and tubes are presented first, followed by the forced-convection heat-transfer process, PFL hardware, working fluids, engineering design guidelines, computer-analysis tools, and the application of a PFL on the Mars Pathfinder spacecraft. Providing all applicable details and analytical equations for PFL design would be impossible; therefore, numerous references are listed at the end of this chapter.

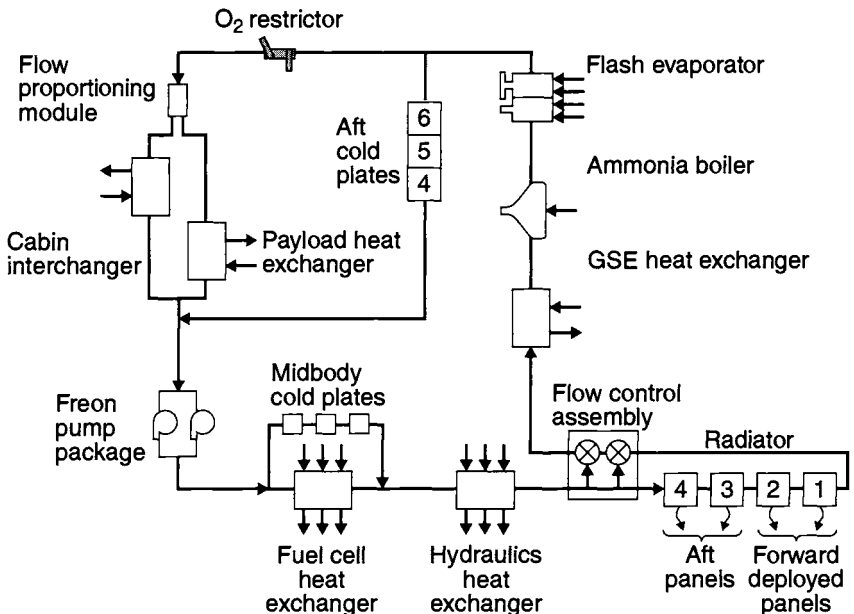


Fig. 12.2. Orbiter ATC system.

Fluid-Flow Concepts and Basic Equations

General

The various components (pump, heat exchanger, radiator, etc.) within a PFL system are connected mainly by conduits. The flows through pipes or tubes may be laminar or turbulent. The pipe-flow regime is primarily a function of the Reynolds number, $Re = \rho VD/\mu$, where ρ is the density of the fluid, V the average flow velocity, D the pipe diameter, and μ the dynamic viscosity of the fluid. A critical Reynolds number distinguishes the flow regimes between laminar or turbulent flow in pipes. The flow becomes turbulent when $Re > 2300$. However, a range of Reynolds numbers for transition flow has been observed experimentally. Depending on the pipe roughness and smoothness, the flow changes from laminar to turbulent in the range of the Reynolds numbers from 2000 to 4000.

In the study of fluid flow in a piping system, the conservation principles are used to set up the governing equations. These principles are the conservation of mass, the conservation of momentum, and the conservation of energy. The following sections briefly present some basic equations used in pipe-flow analysis.

Fundamentals of Pipe Flow

Continuity Equation

Consider steady flow through a portion of the stream pipe; the principle of conservation of mass states that the net mass outflow from section 1 to 2 of the control volume must be zero. Since no flow occurs through the wall of the stream pipe, the continuity equation for one-dimensional flow in a pipe can be written as

$$\dot{m} = \rho_1 V_1 A_1 = \rho_2 V_2 A_2, \quad (12.1)$$

where the subscripts 1 and 2 refer to the flow parameters at the inlet and the outlet, respectively; \dot{m} is the mass flow rate; V the mean velocity; and A the cross-sectional area.

Bernoulli's Equation

Steady-state one-dimensional internal flow is generally known as internal pipe flow, and the equation that governs it is called Bernoulli's equation. A flow network is simulated by specifying flow-passage connections, which can include pipes, pumps, and valves. Associated with a flow passage are the upstream and downstream pressures, and the characteristics that govern the pressure drop.

The pressure drop across a pipe is given by Bernoulli's equation. The general form of this equation, including head loss resulting from irreversibilities for pipe flow along a streamline, is

$$\left(\frac{P_1}{\rho} + \frac{V_1^2}{2} + gZ_1 \right) - \left(\frac{P_2}{\rho} + \frac{V_2^2}{2} + gZ_2 \right) = h_l, \quad (12.2)$$

where subscripts 1 and 2 refer to the flow parameters at the inlet and outlet; P is pressure; V is average fluid velocity; ρ is density; g is the gravitational constant; Z

is elevation; and h_{l_t} is total head loss. This equation shows that the total head loss is the difference in potential energy, flow energy, and kinetic energy. The importance of the total head loss will be discussed in detail in the next section.

Head Loss

The main purpose of analysis of flow in pipes and tubes is to evaluate the pressure changes that result from incompressible flow in the system. The pressure changes in a flow system result from friction and changes in elevation and flow velocity. In a frictionless flow, the Bernoulli equation could account for the effects of changes in elevation and flow velocity. In a real flow, analysis must also include the effect of friction. This effect acts to decrease the pressure, causing such a case, unlike the frictionless flow case, to exhibit a pressure "loss." This pressure loss, h_{l_t} (total head loss) in Eq. (12.2), contains two constituents: the major head loss, h_l (resulting from friction in fully developed flow in constant-area portions of the system), and the minor head loss, h_{l_m} (resulting from frictional effects in flow-through valves, tees, elbows, and other nonconstant-area parts of the system). Thus, the total head loss h_{l_t} in a piping system can be defined as

$$h_{l_t} = h_l + h_{l_m}, \quad (12.3)$$

where h_l is the major head loss and h_{l_m} is the minor head loss.

The details of the major and minor losses in fluid flow are discussed in the following section.

Major Losses

Flow through a piping system causes a reduction in static head, which may be expressed in terms of velocity head $V^2/2$. The major head loss is given by

$$h_l = f \frac{L}{D} \cdot \frac{V^2}{2}, \quad (12.4)$$

where L and D are the length and diameter of the pipe, respectively. The friction factors are

$$f = \frac{64}{Re} \quad (12.5)$$

for laminar flow, and for turbulent flow in smooth pipes:^{12.1–12.3}

$$f = \frac{0.079}{Re^{0.25}} \quad 4 \times 10^3 < Re < 2 \times 10^4 \quad (12.6)$$

$$f = \frac{0.184}{Re^{0.2}} \quad 2 \times 10^4 < Re < 3 \times 10^5 \quad (12.7)$$

$$f = \frac{0.046}{Re^{0.2}} \quad 2 \times 10^4 < Re < 10^6 \quad (12.8)$$

$$f = \frac{1}{[1.581 \ln(Re) - 3.28]^2} \quad 10^4 < Re < 10^7 \quad (12.9)$$

In laminar flow, the friction factor is a function of the Reynolds number only; it is independent of roughness. The widely used frictional factor f is determined from empirical correlation of the Moody diagram,^{12.4} shown in Fig. 12.3 as

$$f = \frac{0.25}{\left[\log \left(\frac{\frac{\varepsilon}{D}}{3.7} + \frac{5.74}{Re^{0.9}} \right) \right]^2}, \quad (12.10)$$

where $Re (= \rho VD/\mu)$ is the Reynolds number, μ is the dynamic viscosity, and ε/D is the relative roughness. The choice of the cutoff Reynolds number between the two regimes (laminar and turbulent) is somewhat arbitrary.

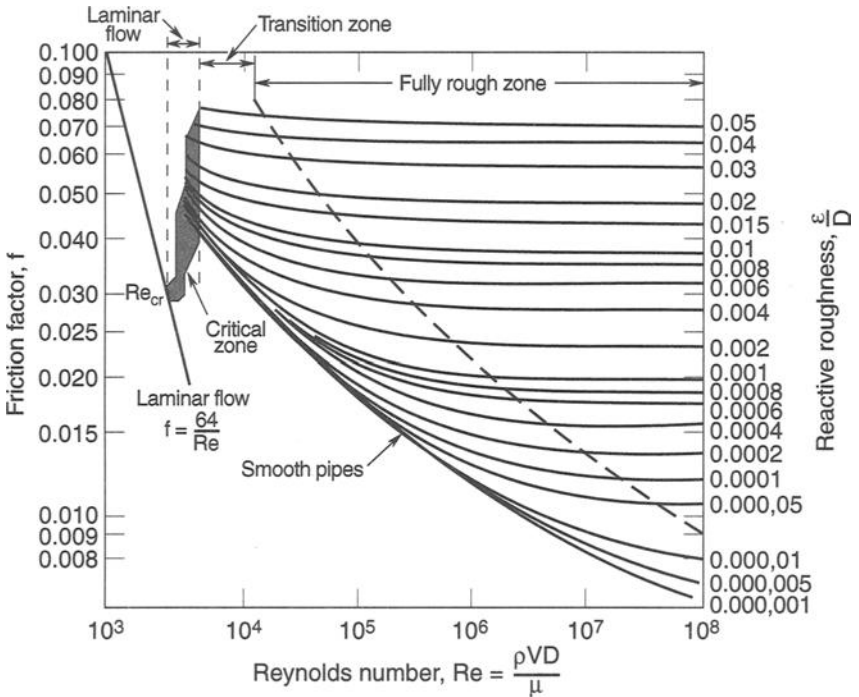


Fig. 12.3. Friction factor for fully developed flow in circular pipes.

Minor Losses

Flow in a piping system may be required to pass through a variety of fittings, bends, or abrupt changes in area, which usually results in flow separation. Energy in the fluid is dissipated by the mixing of fluid in the separated zones. This results in additional head losses, which are primarily the results of flow separation. These losses are small compared to the frictional losses and are, therefore, called minor losses. The minor head loss may be expressed by either

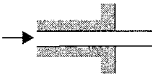
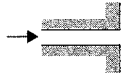
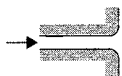
$$h_{l_m} = K \frac{V^2}{2} \quad (12.11)$$

or

$$h_{l_m} = f \frac{L_e}{D} \cdot \frac{V^2}{2}, \quad (12.12)$$

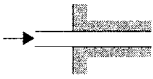
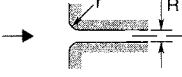
where L_e is the equivalent length, and K , the loss coefficient, must be determined experimentally for each situation. Loss coefficients for various types of entrances and exits are shown in Tables 12.1 and 12.2. Minor loss coefficients for sudden area changes (enlargements and contractions) are given in Table 12.3 and Figs. 12.4 and 12.5.

Table 12.1. Loss Coefficients for Pipe Exits^a

Exit Type	Diagram	Loss Coefficient (K)
Projecting pipe		1.0
Square-edged		1.0
Rounded		1.0

^aBased on $h_{l_m} = K(\bar{V}^2/2)$, calculation of head loss.

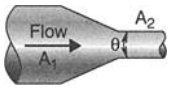
Table 12.2. Loss Coefficients for Pipe Entrances

Entrance Type	Diagram	Loss Coefficient (K) ^a
Re-entrant		0.78
Square-edged		0.34
Slightly rounded		0.2–0.25
Well rounded ^b		0.04

^aBased on $h_{l_m} = K(\bar{V}^2/2)$, where \bar{V} is the mean velocity in the pipe.

^b $r/R = 0.35$.

Table 12.3. Loss Coefficients for Gradual Contractions

Diagram	Included Angle, θ (deg)	Loss Coefficient, K ^a
	30	0.02
	45	0.04
	60	0.07

^aBased on $h_{l_m} = K(\bar{V}^2/2)$.

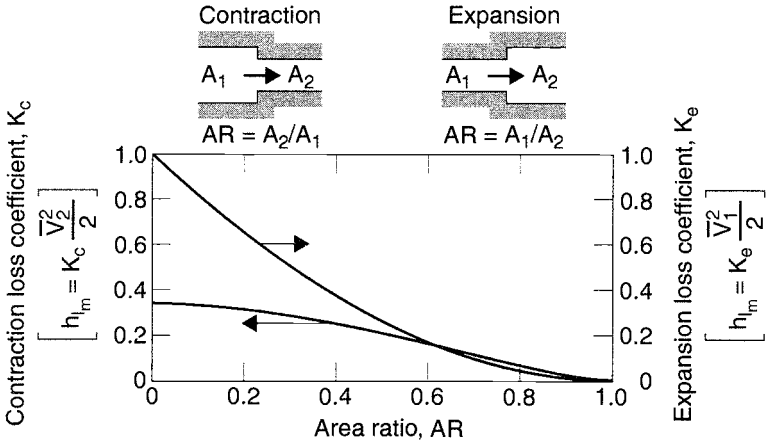


Fig. 12.4. Loss coefficients for flow through sudden area changes.

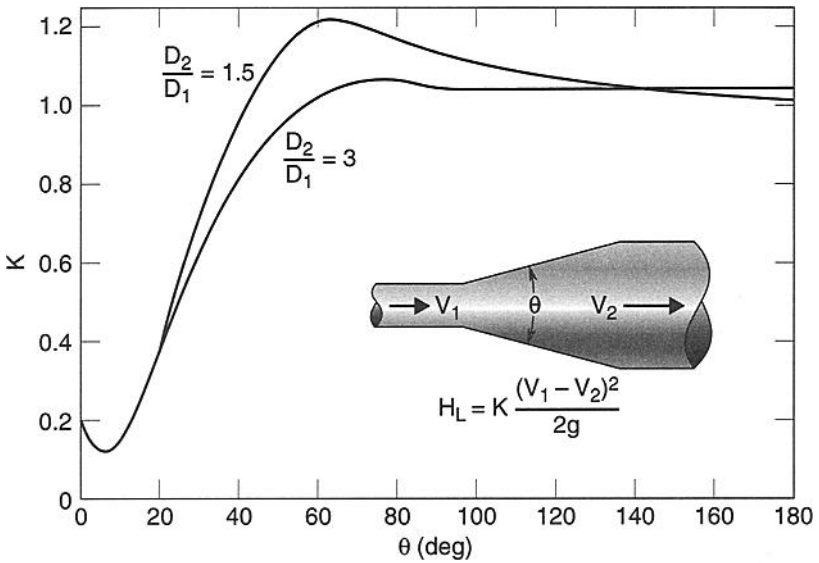


Fig. 12.5. Loss coefficients for conical expansions.

The minor loss of a pipe bend is normally expressed by an equivalent length of straight pipe. The equivalent lengths of a 90-deg pipe bend and miter bend are shown in Figs. 12.6 and 12.7. The representative equivalent lengths for valves and fittings are also given in Table 12.4.

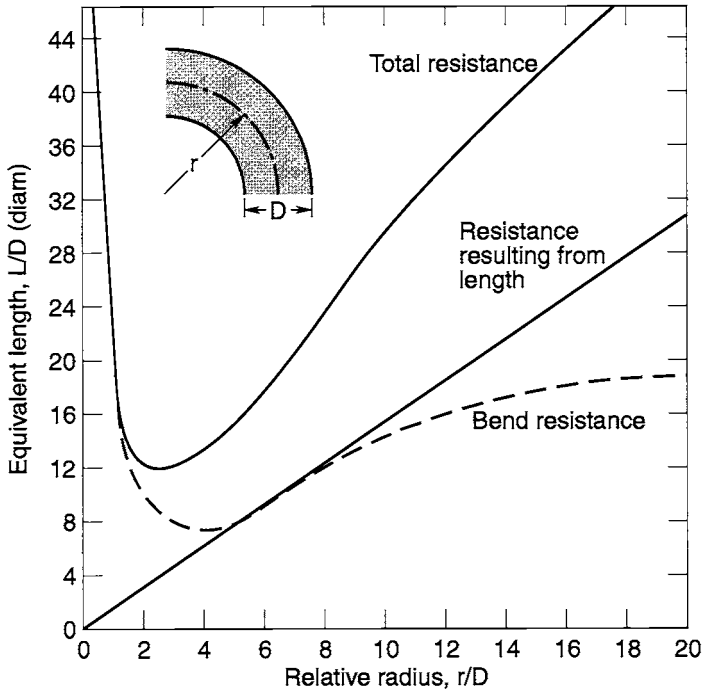


Fig. 12.6. Design chart resistance of 90-deg bends in circular pipe with fully developed turbulent flow.

Friction Factor and Pressure Drop

The Bernoulli equation can be interpreted as the difference of energy per unit weight between two points on a streamline. The change of kinetic energy is usually small compared to the total head loss. Hence, it will be neglected in the evaluation of the pressure drop. Using Eq. (12.2), one can state the pressure drop across a pipe as

$$P_2 - P_1 = \frac{\rho h_f}{g_c} - \frac{\rho g}{g_c}(Z_2 - Z_1). \quad (12.13)$$

By using Eqs. (12.3), (12.4), and (12.11) in Eq. (12.13), one finds that the pressure drop across a pipe becomes

$$P_2 - P_1 = -\frac{\rho V^2}{2g_c} \left(f \frac{L}{D} + K \right) - \frac{\rho g}{g_c}(Z_2 - Z_1), \quad (12.14)$$

where g_c is a conversion factor. The value of g_c is 32.2 ft·lbm/lbf·sec² in the British Gravitational System, 1 kg·m/N·sec² in the *Système Internationale d'Unites* (SI) System, and 1 gm·cm/dyne·sec² in the Absolute Metric System.

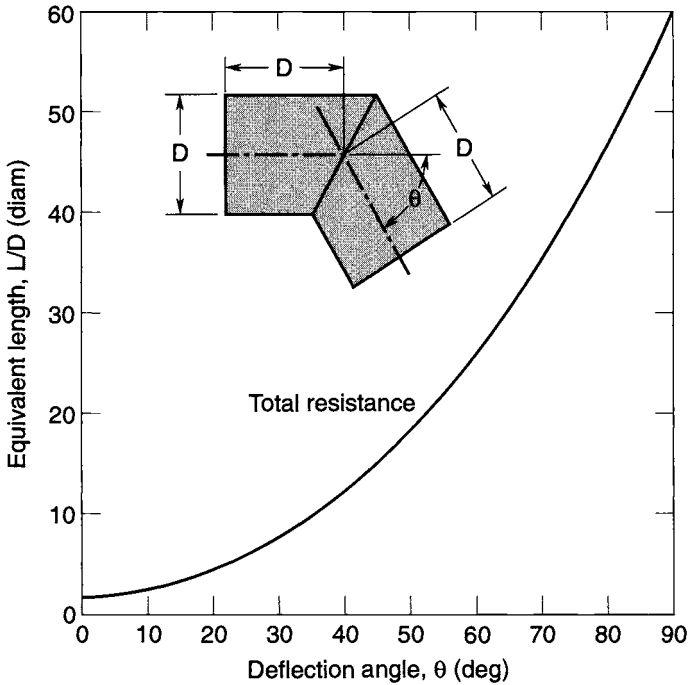


Fig. 12.7. Design chart resistance of miter bends in circular pipe with fully developed turbulent flow.

Table 12.4. Representative Equivalent Lengths in Pipe Diameters (L_e/D) for Valves and Fittings

Fitting Type	Description	Equivalent Length (L_e/D) ^a
Globe valve	Fully open	350
Gate valve	Fully open	13
	3/4 open	35
	1/2 open	160
	1/4 open	900
Check valve		50–100
90-deg std. elbow		30
45-deg std. elbow		16
90-deg elbow	Long radius	20
90-deg elbow		50
45-deg street elbow		26
Tee	Flow-through run	20
	Flow-through branch	60
Return bend	Close pattern	50

^aBased on $h_{l_m} = f \frac{L_e}{D} \cdot \frac{\bar{V}^2}{2}$.

Incorporating the continuity equation, Eq. (12.1), one can rewrite Eq. (12.14) as

$$P_2 - P_1 = -\frac{\dot{m}^2}{2\rho A^2 g_c} \left(f \frac{L}{D} + K \right) - \frac{\rho g}{g_c} (Z_2 - Z_1). \quad (12.15)$$

The equation shows that the pressure drop across a piping system is the sum of the elevation difference of the two points under consideration and the total head loss. In the case of neglecting the elevation change and the minor loss, Eq. (12.14) can be rewritten as

$$\Delta P = P_2 - P_1 = -\frac{\rho V^2}{2g_c} f \frac{L}{D}. \quad (12.16)$$

Forced Convection in Pipes and Tubes

General

In convective heat transfer in internal flow in pipes or tubes, an axially local heat-transfer coefficient h_x is customarily defined as

$$q_x = h_x (T_w - T_b), \quad (12.17)$$

where T_w and T_b are the mean pipe-wall temperature and the fluid-bulk mean temperature, respectively. The flow-length average heat-transfer coefficient \bar{h} is the integrated average of h_x for the total of the pipe from $x = 0$ to $x = L$,

$$\bar{h} = \frac{1}{L} \int_0^L h_x dx. \quad (12.18)$$

For convenience, the heat-transfer coefficient is commonly related to the dimensionless Nusselt number in convective heat transfer. The Nusselt number, by definition, is the ratio of the convective conductance, h , to the molecular thermal conductance, k/D . The local Nusselt number, Nu_x , is then expressed by

$$Nu_x = \frac{h_x D}{k}. \quad (12.19)$$

The mean flow-length-average Nusselt number based on \bar{h} is defined as

$$Nu_D = \frac{\bar{h} D}{k} = \frac{1}{L} \int_0^L Nu_x dx. \quad (12.20)$$

When the effects of axial heat conduction, viscous dissipation, and flow work are neglected within the fluid, the heat transfer within the system can be evaluated by Eq. (12.21).

$$q = \bar{h}(T_w - T_b) = \left(\frac{Nu_D k}{D}\right)(T_w - T_b). \quad (12.21)$$

Heat Transfer in Laminar Tube Flow

Let $T(r, z)$ be the temperature distribution in the fluid, where r and z are the radial and axial coordinates, respectively. The heat flux from the fluid to the tube wall is governed by Fourier's law of heat conduction,

$$q(z) = -k \left[\frac{\partial T(r, z)}{\partial r} \right]_{\text{wall}}, \quad (12.22)$$

where k is the thermal conductivity of fluid. Combining Eq. (12.22) with Newton's law of cooling, Eq. (12.17), one can write the heat-transfer coefficient in terms of the dimensionless temperature gradient as

$$h = -k \left[\frac{\partial q(r)}{\partial r} \right]_{\text{wall}}. \quad (12.23)$$

The temperature profile for flow inside a circular tube can be obtained by performing an energy analysis on a fluid element.^{12.8–12.10} From knowledge of the temperature profile, the heat-transfer coefficient may be shown to be of the form^{12.11}

$$Nu_D = \frac{hD}{k} = 4.364 \quad \text{for uniform heat flux at the tube wall,} \quad (12.24)$$

and

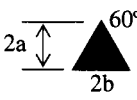
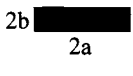
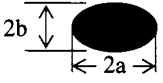
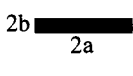
$$Nu_D = \frac{hD}{k} = 3.66 \quad \text{for constant tube-wall temperature.} \quad (12.25)$$

The Nusselt number for laminar flow inside a circular tube was given above for two different boundary conditions, namely, the constant wall temperature and the constant wall heat flux. Shah and London^{12.12} have compiled a list of Nusselt numbers and the quantities $f \cdot Re$ (i.e., the product of the friction factor and the Reynolds number) for geometries other than the circular tube and parallel plates for the above boundary conditions. The results are listed in Table 12.5.

The Nusselt number and the friction factor for laminar flow in ducts of various cross sections have been determined in the region where velocity and temperature profiles are fully developed. If the duct cross section for flow is not circular, then the heat transfer and friction factor, for many cases of practical interest, can be based on the hydraulic diameter, D_h , defined as

$$D_h = \frac{4A_c}{P}, \quad (12.26)$$

Table 12.5. Nusselt Number and Friction Factor for Fully Developed Laminar Flow in Ducts of Various Cross Sections (Ref. 12.9)

Geometry ($L/D_h > 100$)	Nu_T^a	Nu_H^b	Nu_H^c	fRe
	3.657	4.364	4.364	64.00
 $\frac{2b}{2a} = \frac{\sqrt{3}}{2}$	2.470	3.111	1.892	53.33
	3.340	4.002	3.862	60.22
 $\frac{2b}{2a} = 1$	2.976	3.608	3.091	56.91
 $\frac{2b}{2a} = \frac{1}{2}$	3.391	4.123	3.017	62.20
 $\frac{2b}{2a} = \frac{1}{4}$	3.660	5.099	4.35	74.80
 $\frac{2b}{2a} = 0.9$	4.439	5.331	2.930	72.93
 $\frac{2b}{2a} = \frac{1}{8}$	5.597	6.490	2.904	82.34
 $\frac{2b}{2a} = 0$	7.541	8.235	8.235	96.00
 Insulated $\frac{b}{a} = 0$	4.861	5.385	—	96.00

^aNusselt number for uniform wall temperature.

^bNusselt number for uniform wall heat flux in the flow direction while the wall temperature remains uniform around the periphery.

^cNusselt number for uniform wall heat flux both in the flow direction and around the periphery.

where A_c and P are the cross-sectional flow area and the wetted perimeter, respectively. This diameter is the one that should be used in the calculation of the Nusselt and Reynolds numbers.

Heat Transfer in Turbulent Tube Flow

A classical expression for computing the local Nusselt number for fully developed turbulent flow in a smooth circular tube can be obtained from the Chilton-Colburn analogy. The analogy relates the local drag coefficient C_f to the local Stanton number St ($= Nu/Re \cdot Pr$) in the form

$$StPr^{2/3} = \frac{C_f}{2} = \frac{f}{8}, \quad (12.27)$$

where Pr ($= \nu/\alpha$) is the Prandtl number, the ratio of kinematic viscosity and thermal diffusivity of a fluid, which represents the relative magnitudes of diffusion and heat conduction in the fluid medium. Substituting the friction factor from Eq. (12.7) into Eq. (12.27) yields the Colburn equation for turbulent flow inside a smooth tube:

$$Nu = 0.023Re^{0.8}Pr^{1/3}. \quad (12.28)$$

Eq. (12.28) is applicable for $0.7 < Pr < 160$, $Re > 10,000$, and $L_e/D > 60$ for smooth tubes. A large number of empirical correlations have been developed by many investigators in the past to determine the heat-transfer coefficient; some are presented in Table 12.6.

System Hardware

Pumps

General

A pump is a machine that adds energy to liquid. It converts kinetic energy into pressure potential. A pump consumes more power than it gives off because of internal friction losses. Some major losses include hydraulic losses (flow friction and turbulence) and mechanical losses (friction in bearings and other internal mechanical parts). Depending on their design and mechanical action, most pumps used in space applications can be classified into one of the following categories:^{12,21}

- **Rotodynamic.** These pumps add energy to a liquid medium through the work done by a rapidly rotating vaned impeller. The radial-flow centrifugal pumps, mixed-flow pumps, axial-flow pumps, and propellers can be classified as rotodynamic pumps. Some typical rotodynamic pumps are shown in Table 12.7.
- **Displacement.** This category includes the reciprocating (Table 12.8) and rotary (Table 12.9) pumps. These pumps impart energy by a positive displacement action.

Table 12.6. Summary of Correlations for Forced-Convection Turbulent Flow inside Duct^a

Correlation	Remarks
$f = (1.82 \log Re - 1.64)^{-2}$	Smooth tubes, $Re > 10^4$
$f = 0.316 Re^{-0.25}$	Smooth tubes, $Re < 2 \times 10^4$
$f = 0.184 Re^{-0.2}$	Smooth tubes, $2 \times 10^4 < Re < 3 \times 10^5$
$Nu = 0.023 Re^{0.8} Pr^{1/3}$	$0.7 < Pr < 160$; $Re > 10,000$; $L/D > 60$; smooth pipes
$Nu = 0.023 Re^{0.8} Pr^n$ $n = 0.4$ for heating $n = 0.3$ for cooling	$0.7 < Pr < 160$; $Re > 10,000$; $L/D > 60$; smooth pipes
$Nu = 0.027 Re^{0.8} Pr^{1/3} \left(\frac{\mu_b}{\mu_w}\right)^{0.14}$	$0.7 < Pr < 16,700$; $Re > 10,000$; $L/D > 60$; smooth pipes
$Nu = \frac{Re Pr}{X} \left(\frac{f}{8}\right) \left(\frac{\mu_b}{\mu_w}\right)^n$ where: $X = 1.07 + 12.7 (Pr^{2/3} - 1)(f/8)^{1/2}$ $n = 0.11$ heating with uniform T_w $n = 0.2$ cooling with uniform T_w $n = 0$ uniform wall heat flux or gases	Smooth or rough pipes $10^4 < Re < 5 \times 10^6$ $0.5 < Pr < 200$ with 5 to 6% error $0.5 < Pr < 2000$ with 10% error Properties, except m_w , are evaluated at bulk mean temperature.
$Nu = 0.036 Re^{0.8} Pr^{1/3} \left(\frac{D}{L}\right)^{0.055}$	$10 < \frac{L}{D} < 400$
$Nu = 5 + 0.016 Re^c Pr^d$ where: $c = 0.88 - \frac{0.24}{4 + Pr}$ $d = 0.33 + 0.5e^{-0.6Pr}$	$0.1 < Pr < 10^4$ $10^4 < Re < 10^6$ $\frac{L}{D} > 25$

^aSubscript *b* indicates fluid properties evaluated at the bulk mean temperature; subscript *w* indicates fluid properties evaluated at the wall temperature.

The European Space Agency^{12.21} has compiled a list of some important features of the rotodynamic and displacement pumps; the information is contained in Table 12.10. The following requirements are normally imposed on pumps for space-application fluid loops:

- high efficiency
- low mass
- relatively low mass-to-output-power ratio
- hermetically sealed structure
- minimum operational noise level
- ability to withstand mission vibration and shock loads
- compatibility with onboard electrical system
- applicability to aerospace-environment usage
- ability to handle typical liquid coolants as working fluids
- high operational reliability

Table 12.7. Rotodynamic Pumps

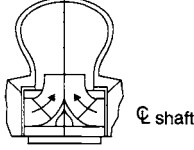
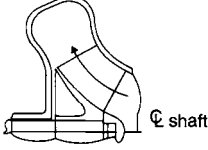
Class	Typical Model
Radial flow	
Mixed flow	
Axial flow or propeller	

Table 12.8. Reciprocating Displacement Pumps

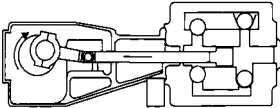
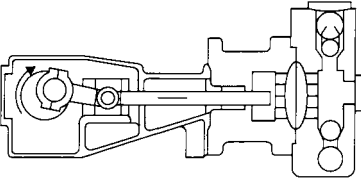
Class	Typical Model
Piston	
Diaphragm	

Table 12.9. Rotary Displacement Pumps

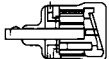
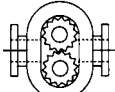
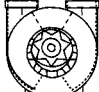
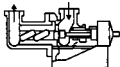
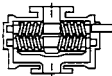
Class	Typical Models		
Vane	 Sliding vane	 External vane	
Piston	 Axial piston		
Flexible member	 Flexible tube	 Flexible vane	 Flexible liner
Gear	 External gear	 Internal gear	
Lobe	 Single lobe	 Treble lobe	
Circumferential piston	 Circumferential piston		
Screw	 Single screw	 Screw and wheel	 Double screw

Table 12.10. Main Features of Typical Pumps^a

Rotodynamic Pumps	Positive-Displacement Pumps
Very efficient when operating at speeds from 1200 to 3600 rpm, within the usual range of alternating-current electric motors.	Operate at very low rotating speed (220 to 500 rpm).
Cannot be run efficiently at low speeds to pump small quantities.	Efficiencies, although they can be high, are below those of rotodynamic pumps.
Overall efficiency usually ranges from 0.7 to 0.85.	Efficiency decreases when wear increases leakage.
Not easily regulated. Regulation by throttling is simple but wasteful. Regulation by running speed adjustment more or less maintains the efficiency but requires auxiliary equipment that is expensive, complicated, and unreliable. Multiple winding motors and invertors are used to control motor speed considerations.	The discharge characteristic is a pulsating one. A smoother discharge is obtained in double- or treble-acting units. Rotary pumps exhibit greater uniformity of delivery than reciprocating pumps.
Cannot deliver at high pressure unless a large and heavy type is used. Pressure rise increases as peripheral speed is increased.	The delivery is substantially constant, regardless of the pressure rise developed.
Cannot handle viscous liquids.	Can be used with very viscous liquids. This feature applies especially to the case of rotary pumps. The pressure rise drops with increasing viscosity.
Not self-priming, although that limitation can be overcome in various ways.	Self-priming and capable of coping with high-suction lifts.
No relief valves are to be used. Even complete throttling does not present any danger to the pump or loop, as no further pressure rise develops.	Relief or bypass valves are to be used. Unable to operate against a closed discharge. Even a slight decrease in delivery may cause a substantial pressure rise.
Limited by cavitation and power.	Able to handle large proportions of vapor. Enough liquid must be present to provide a liquid sealing film for the clearances. Suitable for pumping hot liquid. Limited by pressure and power.
Leak through the shaft seal. Submerged pumps can be used to prevent this drawback.	Problems of leakage are minimized, particularly with diaphragm pumps.
Smaller in size than other types with equal capacity.	Much bigger than rotodynamic pumps because of low rotating speed.
Low-cost, rugged, and reliable in operation.	Complicated construction. Unlike rotary pumps, they require the use of inlet and outlet valves. Very sensitive to wear because comparatively large surface areas move in close contact. Diaphragm pumps do not present friction, but diaphragm materials are of limited use at elevated temperatures.

^aArranged by the compiler (Ref. 12.21) after: Nekrasov (1969), London (1974), Pollak & Cruger (1974), Scoble (1974), Settles *et al.* (1977).

Characteristic Curves

The performance parameters for a typical pump include the pressure head (H), the input power (P), and the machine efficiency (η) under some specific operating conditions. These parameters are the pump-dependent variables. The volumetric flow rate (Q), angular speed (ω), impeller diameter (D), and fluid properties (e.g., density, ρ) are the independent variables. Pump-characteristic curves are generated by plotting a dependent variable as a function of one of the independent variables. Pump performance is difficult to predict analytically except at the design point of the specific machine; hence, it is measured experimentally. Some typical characteristic curves showing head, efficiency, and horsepower as a function of the discharge for a typical centrifugal pump are shown in Fig. 12.8. These curves are shown for a centrifugal pump tested at constant speed. When a pump with performance curves like these is installed in a pumping system, its design operating point is controlled by the so-called system-components (e.g., piping, valves, and fittings) resistance. The system resistance, as defined in Eq. (12.16), is proportional to the square of the velocity. The friction factor and equivalent length vary somewhat with flow rate, accounting for the deviation from a parabolic velocity distribution. The head-capacity curve of a typical pump with the system-resistance curve superimposed is shown in Fig. 12.9 as a function of the volume flow rate. The only possible system operating point is the intersection of these two curves where the head developed by the pump just balances the head loss resulting from friction in the system.

Pump Laws

The basic pump laws are derived using the principles of dynamic similarity and dimensional analysis. "Similarity" in pump design refers to the case of two machines operating under identical flow conditions. The results from the basic pump laws^{12.22} are presented in Eqs. (12.29–12.31).

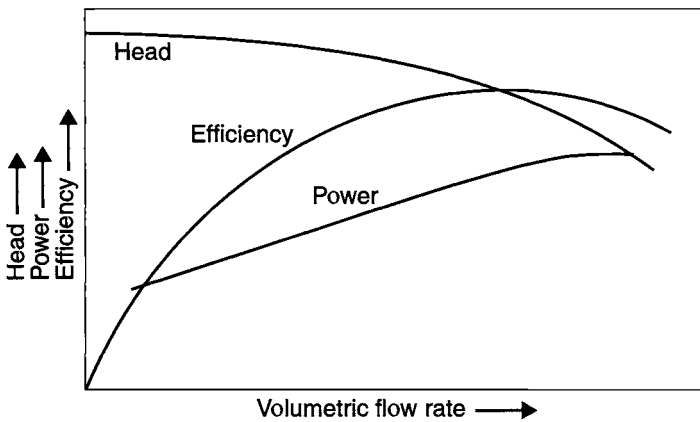


Fig. 12.8. Characteristic curves for a typical centrifugal pump.

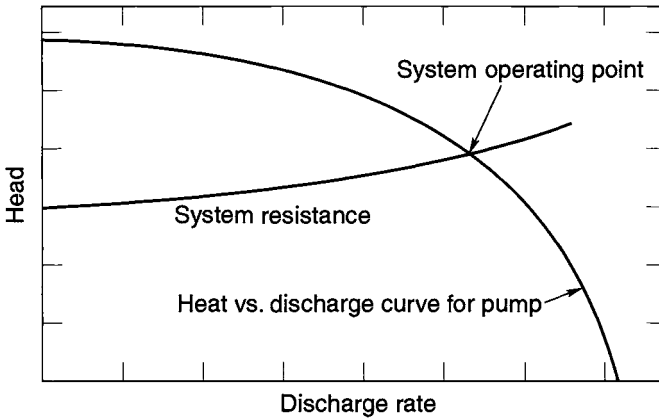


Fig. 12.9. Pump and system curves.

$$\frac{Q_1}{\omega_1 D_1^3} = \frac{Q_2}{\omega_2 D_2^3}, \quad (12.29)$$

$$\frac{H_1}{\omega_1^2 D_1^2} = \frac{H_2}{\omega_2^2 D_2^2}, \quad (12.30)$$

and

$$\frac{P_1}{\rho_1 \omega_1^3 D_1^5} = \frac{P_2}{\rho_2 \omega_2^3 D_2^5},$$

and the specific speed is defined by

$$N_s = \frac{\omega Q^{1/2}}{H^{3/4}}. \quad (12.31)$$

These laws only hold true at different operating conditions as long as the pump efficiency is constant.

Heat Exchangers

Types of Heat Exchangers

The most common heat exchangers fall into three categories:

- **Flat-plate.**
- **Shell-and-tube.** The simplest form is the double-pipe exchanger shown in Fig. 12.10(a). If the hot and cold fluids both flow in the same direction, it is referred to as a parallel-flow type; otherwise, it is a counterflow type. Some common types of shell-and-tube heat exchangers are shown in Fig. 12.10(b).
- **Crossflow.** In this type of exchanger, the two fluids flow at right angles to each other, as shown in Fig. 12.10(c). The flow may be called mixed or unmixed within the crossflow arrangement.

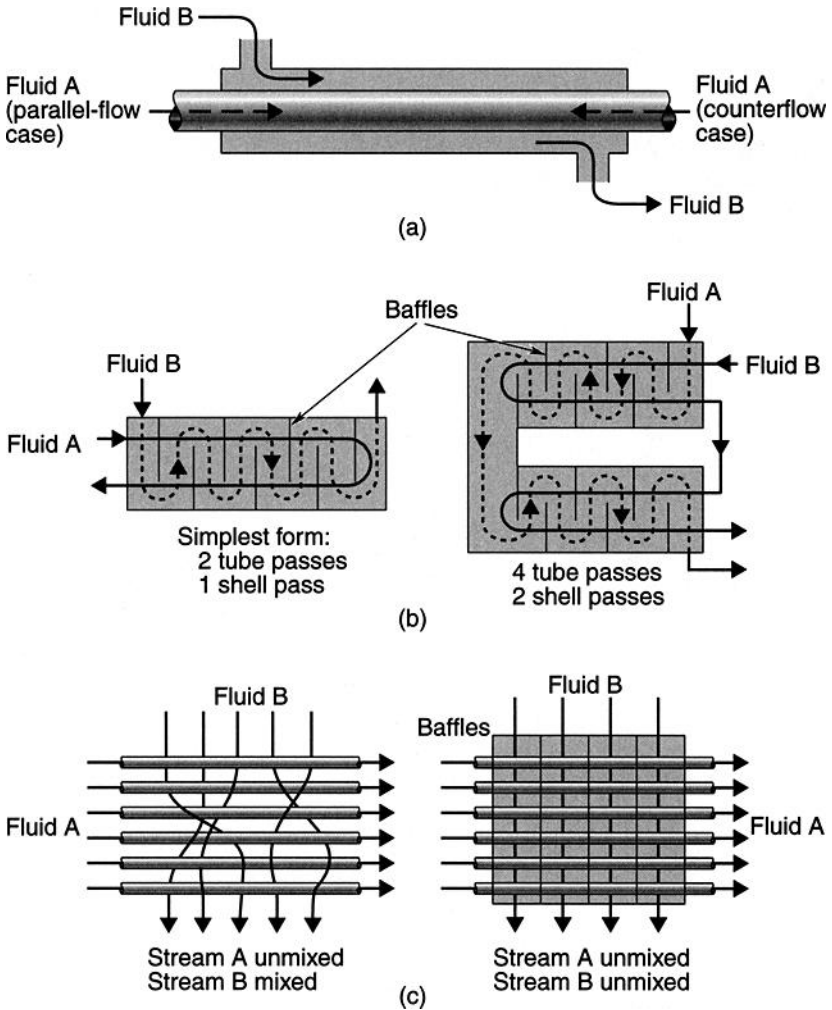


Fig. 12.10. Basic types of heat exchanger. (a) Parallel and counterflow heat exchangers, (b) two kinds of shell-and-tube exchanger, and (c) two kinds of crossflow exchanger.

Heat-Transfer Calculations

The main objective in the thermal design of heat exchangers is to determine the necessary surface area required to transfer heat at a given rate for given fluid temperatures and flow rates. One important factor is the knowledge of the overall heat-transfer coefficient, U , which can be related in the fundamental heat-transfer relation in Eq. (12.32).

$$Q = UA(\Delta T_m), \tag{12.32}$$

where A represents surface area for heat transfer consistent with the definition of U , and ΔT_m is the mean temperature difference across the heat exchanger.

Overall Heat-Transfer Coefficient. The overall heat-transfer coefficient, U , is proportional to the reciprocal of the sum of the thermal resistances. Consider a wall exposed to a hot fluid A on one side and cooler fluid B on the other side. Some common configurations include a plane wall:

$$U = \frac{1}{\frac{1}{h_o} + \frac{L}{K} + \frac{1}{h_i}},$$

and a cylindrical wall:

$$U_o = \frac{1}{\frac{r_o}{r_i h_i} + \frac{r_o}{k} \ln\left(\frac{r_o}{r_i}\right) + \frac{1}{h_o}}, \quad U_i = \frac{1}{\frac{1}{h_i} + \frac{r_i}{k} \ln\left(\frac{r_o}{r_i}\right) + \frac{r_i}{r_o h_o}}$$

here subscripts i and o represent the inside and outside surfaces of the wall.

Log-Mean Temperature Difference (LMTD). The mathematical expression for the LMTD can be derived by considering a parallel-flow flat-plate exchanger, the temperature profiles of which are shown in Fig. 12.11. From an energy balance on a differential fluid element with length dx for each fluid, the mean temperature ΔT_m for either parallel or counterflow can be determined from the expression in Eq. (12.33).

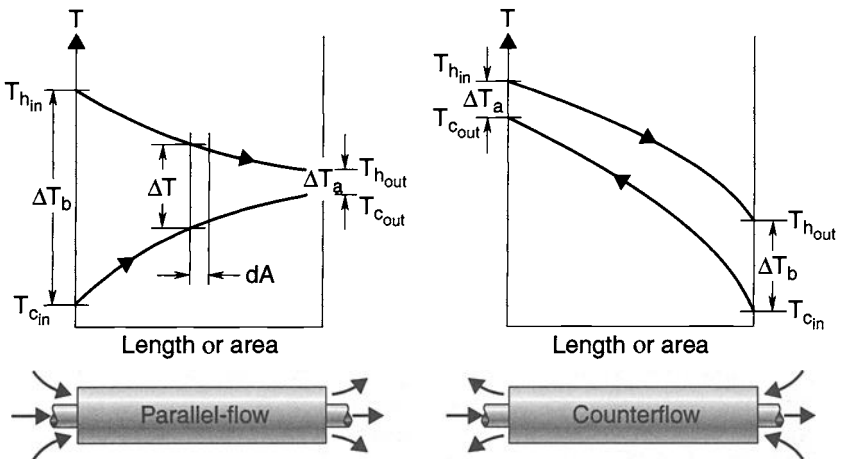


Fig. 12.11. The temperature variation through single-pass heat exchangers.

$$Q = UA\Delta T_m = UA \left[\frac{\Delta T_a - \Delta T_b}{\ln \left(\frac{\Delta T_a}{\Delta T_b} \right)} \right]. \quad (12.33)$$

Thus, the average effective temperature difference ΔT_m in Eq. (12.33) can be written as

$$\Delta T_m = LMTD = \frac{\Delta T_a - \Delta T_b}{\ln \left(\frac{\Delta T_a}{\Delta T_b} \right)}. \quad (12.34)$$

The expression defined by Eq. (12.34) is called the LMTD.

Correction Factors for Complex Heat Exchangers. For more complex heat exchangers, such as those involving multiple tubes, several shell passes, or cross-flow, determination of the average effective-temperature difference is so difficult that the usual practice is to modify Eq. (12.33) by a correction factor, F . Correction factors for several common configurations are given in Fig. 12.12. In these figures the notation (T, t) to denote the temperatures of the two fluid streams has been introduced, since it is immaterial whether the hot fluid flows through the shell or the tubes.

Heat-Exchanger Effectiveness (NTU Method)

The performance of a heat exchanger can be determined once its configuration and the imposed temperature difference are known. However, either the inlet or outlet temperature of the heat exchanger may not be known until the design is complete. An iterative process requiring a trial-and-error approach to finding the heat-transfer rate and the exit temperature is necessary. The so-called effectiveness method developed in full detail by Kays and London in the book *Compact Heat Exchangers* is useful in heat-exchanger design. Heat-exchanger effectiveness is defined as

$$\varepsilon = \frac{\text{actual heat transfer}}{\text{maximum possible heat transfer}} = \frac{Q_{\text{actual}}}{Q_{\text{max}}}. \quad (12.35)$$

The maximum possible heat transfer occurs if one fluid has undergone a temperature change equal to the maximum temperature difference available within the system. This difference is equal to the temperature of the entering hot fluid minus the temperature of the entering cold fluid. The procedure uses the effectiveness ε to eliminate the unknown discharge temperature. As a result, the solution for the heat-exchanger effectiveness becomes a function of the other known system parameters. These include the mass flow rate of the fluid (\dot{m}), heat capacity (c_p), heat-transfer area (A), and the overall heat-transfer coefficient (U). Letting the heat capacitance $C = \dot{m} c_p$, one finds that

$$Q_{\text{actual}} = C_h(T_{hi} - T_{ho}) = C_c(T_{co} - T_{ci}). \quad (12.36)$$

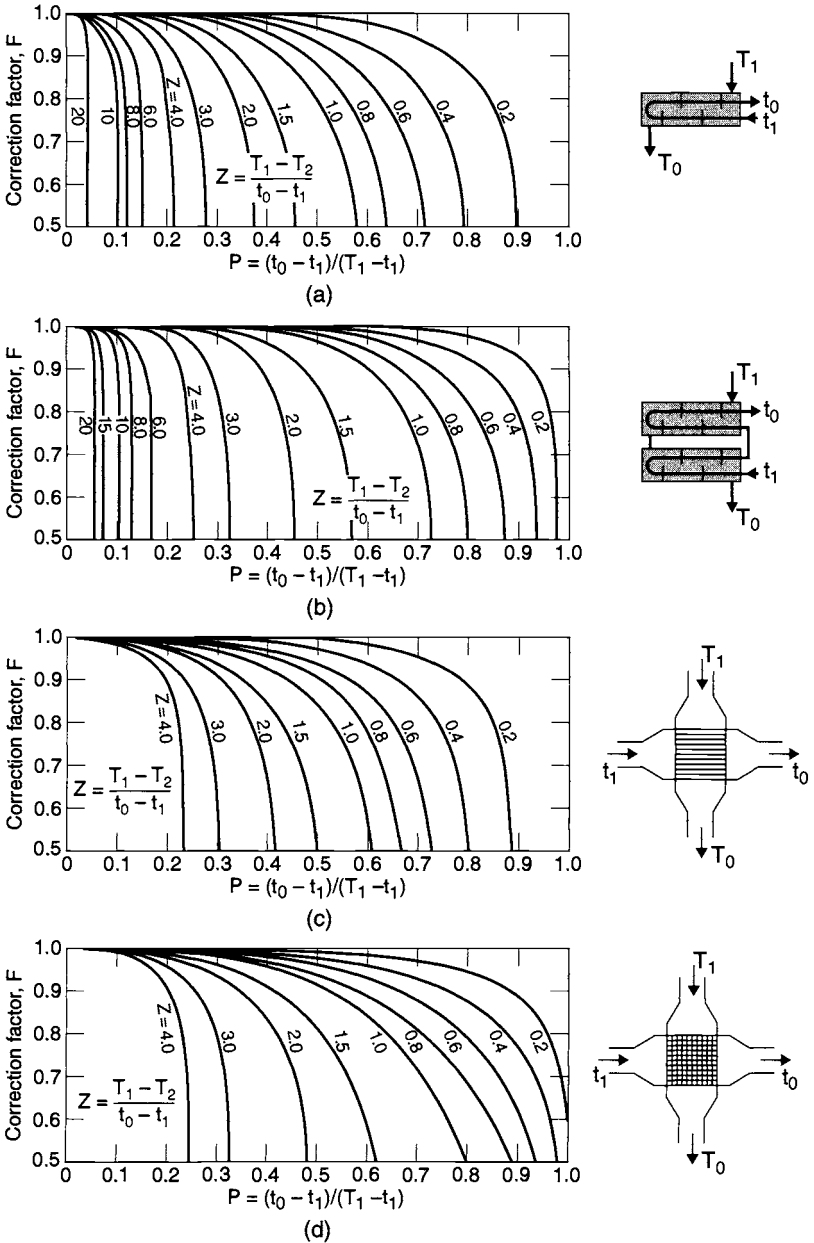


Fig. 12.12. Correction factors for some common heat-exchanger configurations: (a) one shell pass and an even number of tube passes, (b) two shell passes and twice an even number of tube passes, (c) crossflow with one fluid mixed, and (d) crossflow with both fluids unmixed.

Equation (12.36) is an energy balance of both the hot and cold fluids. The maximum possible heat transfer occurs when the fluid of smaller heat capacitance undergoes the maximum temperature variation. This can be stated as

$$Q_{\max} = C_{\min}(T_{hi} - T_{ci}). \quad (12.37)$$

Combining Eqs. (12.36) and (12.37), one determines that in terms of the heat-exchanger effectiveness, actual heat transfer is governed by the equation

$$Q_{\text{actual}} = \varepsilon C_{\min}(T_{hi} - T_{ci}). \quad (12.38)$$

The heat-transfer rate can be determined once the specific value of the heat-exchanger effectiveness is known. The effectiveness (ε) for the parallel single-pass heat exchanger is

$$\varepsilon = \frac{1 - \exp[-(1 + C_{\min}/C_{\max})NTU]}{1 + C_{\min}/C_{\max}}, \quad (12.39)$$

and the corresponding expression for the counterflow case is

$$\varepsilon = \frac{1 - \exp[-(1 - C_{\min}/C_{\max})NTU]}{1 - C_{\min}/C_{\max} \exp[-(1 - C_{\min}/C_{\max})NTU]}, \quad (12.40)$$

where C_{\max} and C_{\min} are the maximum and minimum values of the $C (= \dot{m} c_p)$ for the hot or the cold fluid. Expressions for the effectiveness of other configurations are given in Table 12.11 and Fig. 12.13, where $C = C_{\min}/C_{\max}$. Note that for an evaporator or condenser $C = 0$, because one fluid remains at a constant temperature, making its effective specific heat infinite. The NTU appearing in the last two expressions is the so-called number of heat-transfer units, defined as

$$NTU = \frac{UA}{C_{\min}}. \quad (12.41)$$

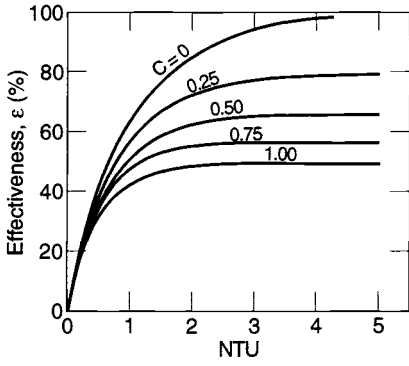
The NTU may be considered as a heat-exchanger size-factor.

Heat-Exchanger Design

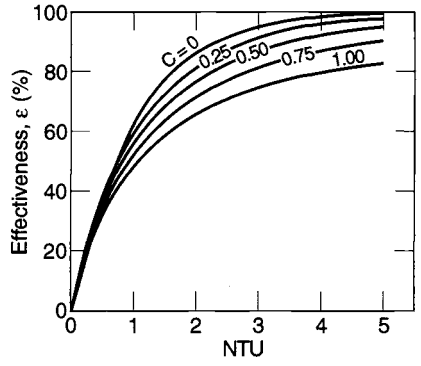
The preceding sections have provided means for predicting heat-exchanger performance. Other considerations in designing heat exchangers are important in addition to the prediction of heat transfer. The primary ones are the minimization of pumping power and the minimization of weight. The weight and size of heat exchangers used in space or aeronautical applications are very important parameters.

Table 12.11. Effectiveness for Various Heat Exchanger Configurations

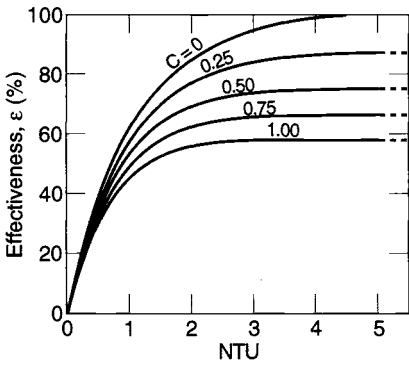
Exchanger Type	Effectiveness	Graph
Parallel-flow: single-pass	$e = \frac{1 - \exp[-NTU(1 + C)]}{1 + C}$	Fig. 12.13(a)
Counterflow: single-pass	$e = \frac{1 - \exp[-NTU(1 - C)]}{1 - C \exp[-NTU(1 - C)]}$	Fig. 12.13(b)
Shell-and-tube (one shell pass; 2, 4, 6, etc., tube passes)	$e_1 = 2 \left[1 + C + \frac{1 + \exp[-NTU(1 + C^2)^{1/2}]}{1 - \exp[-NTU(1 + C^2)^{1/2}]} (1 + C^2)^{1/2} \right]^{-1}$	Fig. 12.13(c)
Shell-and-tube (n shell passes; $2n, 4n, 6n$, etc., tube passes)	$e_n = \left[\left(\frac{1 - e_1 C}{1 - e_1} \right)^3 - 1 \right] \left[\left(\frac{1 - e_1 C}{j - e_1} \right)^3 - C^{-1} \right]$	Fig. 12.13(d) for $n = 2$
Crossflow (both streams unmixed)	$1 - \exp\{C(NTU)^{0.22}[\exp[-C(NTU)^{0.78}] - 1]\}$	Fig. 12.13(e)
Crossflow (both streams mixed)	$e = NTU \left[\frac{NTU}{1 - \exp(-NTU)} + \frac{(NTU)(C)}{1 - \exp[-(NTU)(C)]} - 1 \right]^{-1}$	
Crossflow (stream C_{\min} unmixed)	$e = C \{ 1 - \exp[-C \{ 1 - \exp(-NTU) \}] \}$	Fig. 12.13(f) (dashed curves)
Crossflow (system C_{\max} unmixed)	$e = 1 - \exp\{-C \{ 1 - \exp[-(NTU)(C)] \}\}$	Fig. 12.13(f) (solid curves)



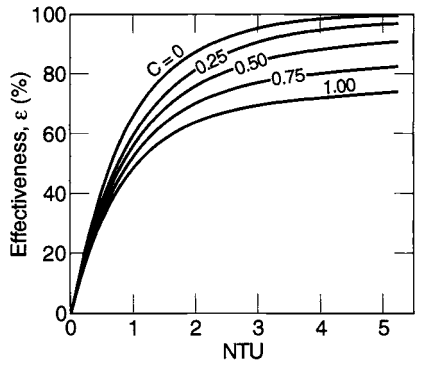
(a)



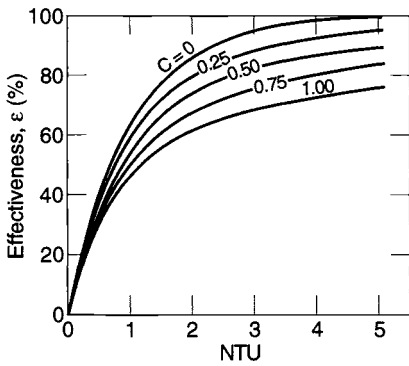
(b)



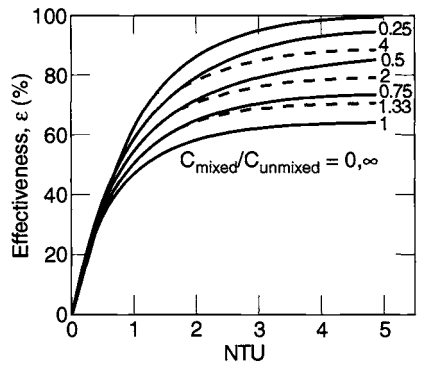
(c)



(d)



(e)



(f)

Fig. 12.13. Heat-exchanger effectiveness.

Working Fluids

The graphs that follow in Figs. 12.14–12.24 show physical properties of some of the most commonly used coolants in heat exchangers. Properties such as vapor pressure (P_{sat}), density (ρ), specific heat (C_p), dynamic viscosity (μ), and thermal conductivity (k) are given. The coolants include:

- Monsanto OS 59 (Fig. 12.14)
- FC 75 (Fig. 12.15)
- Freon E1, E2, E3, E4, E5 (Fig. 12.16)
- Freon 11, 12, 13, 21, 22, 113, 114, 142 (Fig. 12.17)

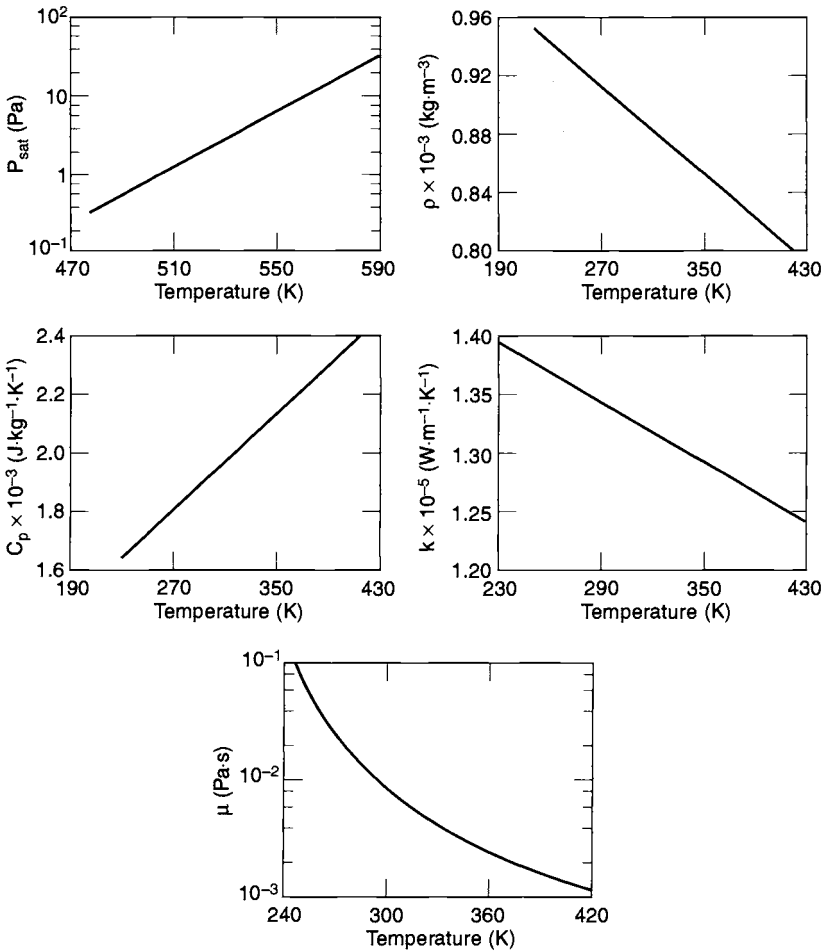


Fig. 12.14. Physical properties of Monsanto OS 59.

- Flutec PP-2, PP-9, PP-50 (Fig. 12.18)
- water/glycol solutions (Fig. 12.19)
- Coolanol 15, 25, 35, 45 (Fig. 12.20)
- carbon tetrachloride (Fig. 12.21)
- water (Fig. 12.22)
- methanol/water solution, DC-200 (Fig. 12.23)
- air (Fig. 12.24)

References 12.49 and 12.59 contain information on other coolants.

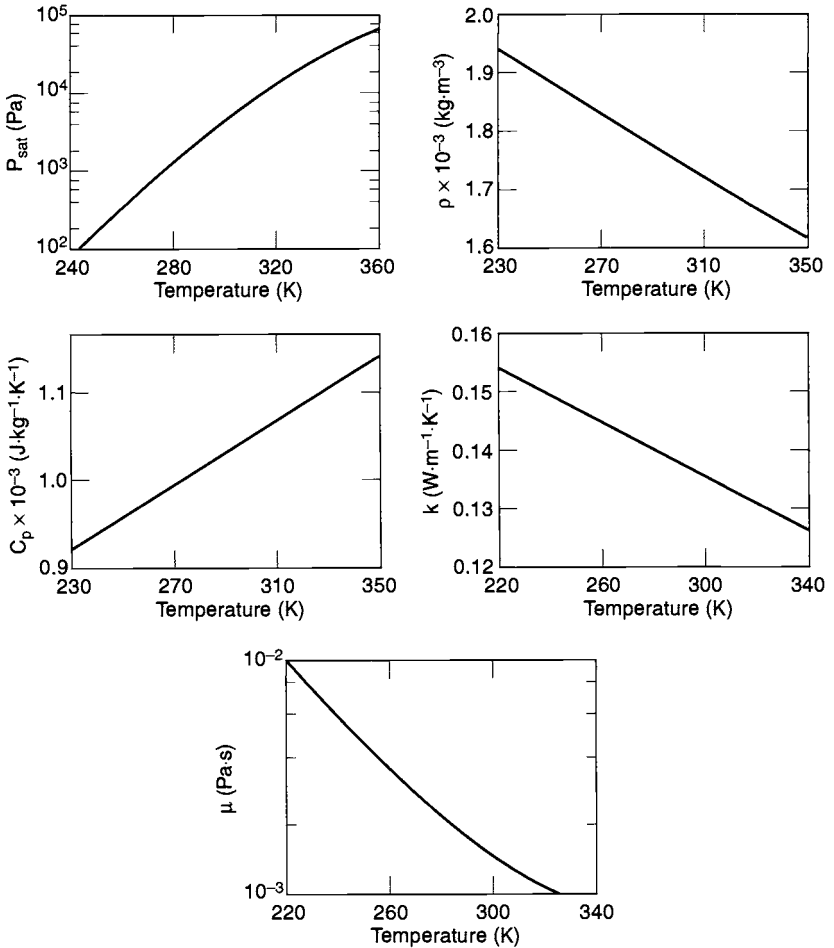


Fig. 12.15. Physical properties of FC 75.

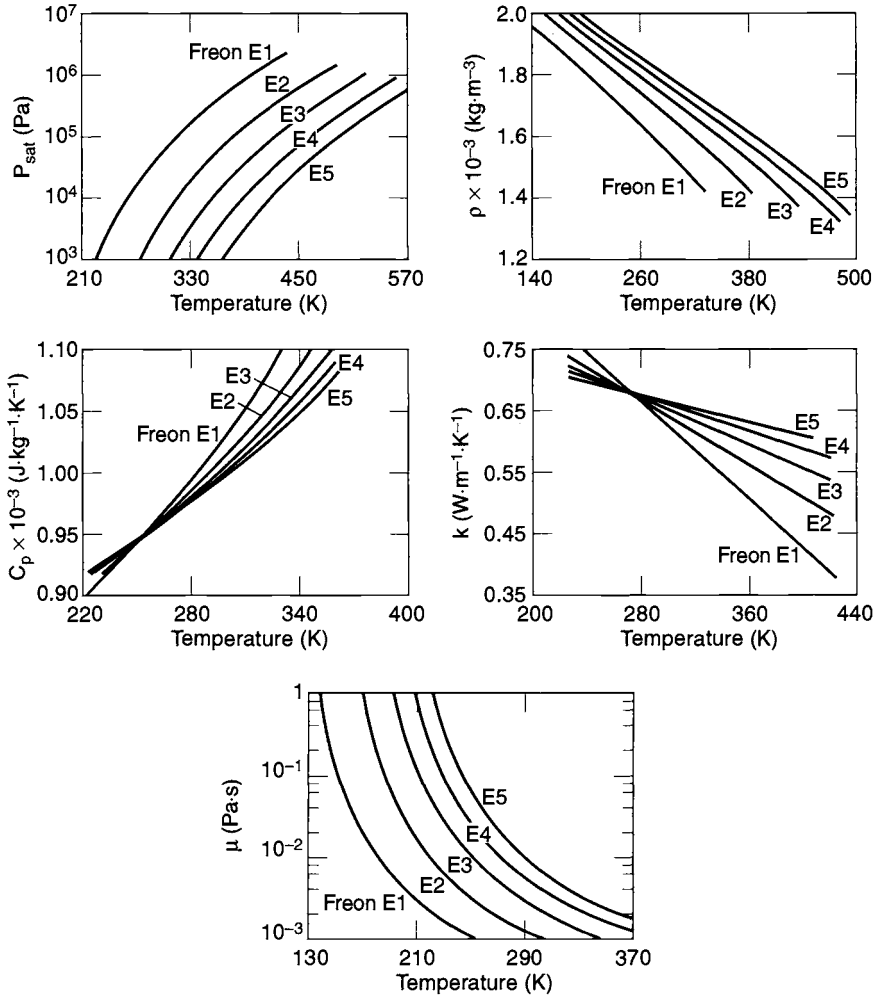


Fig. 12.16. Physical properties of Freon E1, E2, E3, E4, E5.

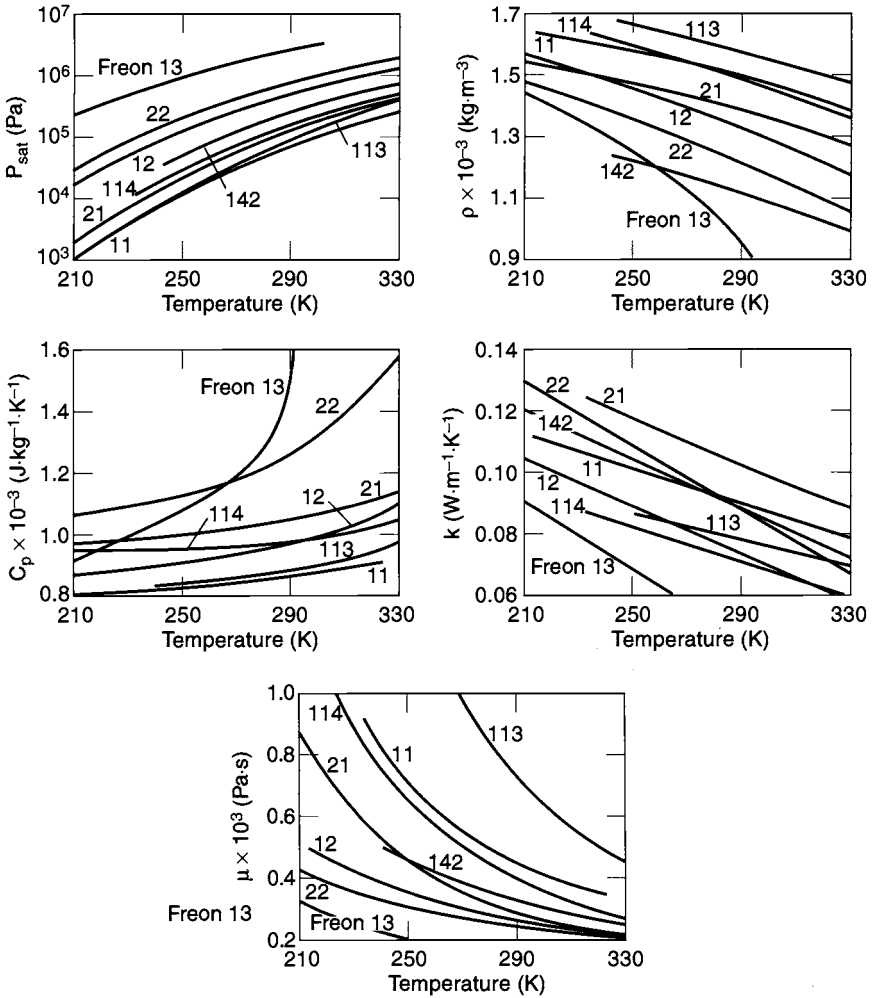


Fig. 12.17. Physical properties of Freon 11, 12, 13, 21, 22, 113, 114, 142.

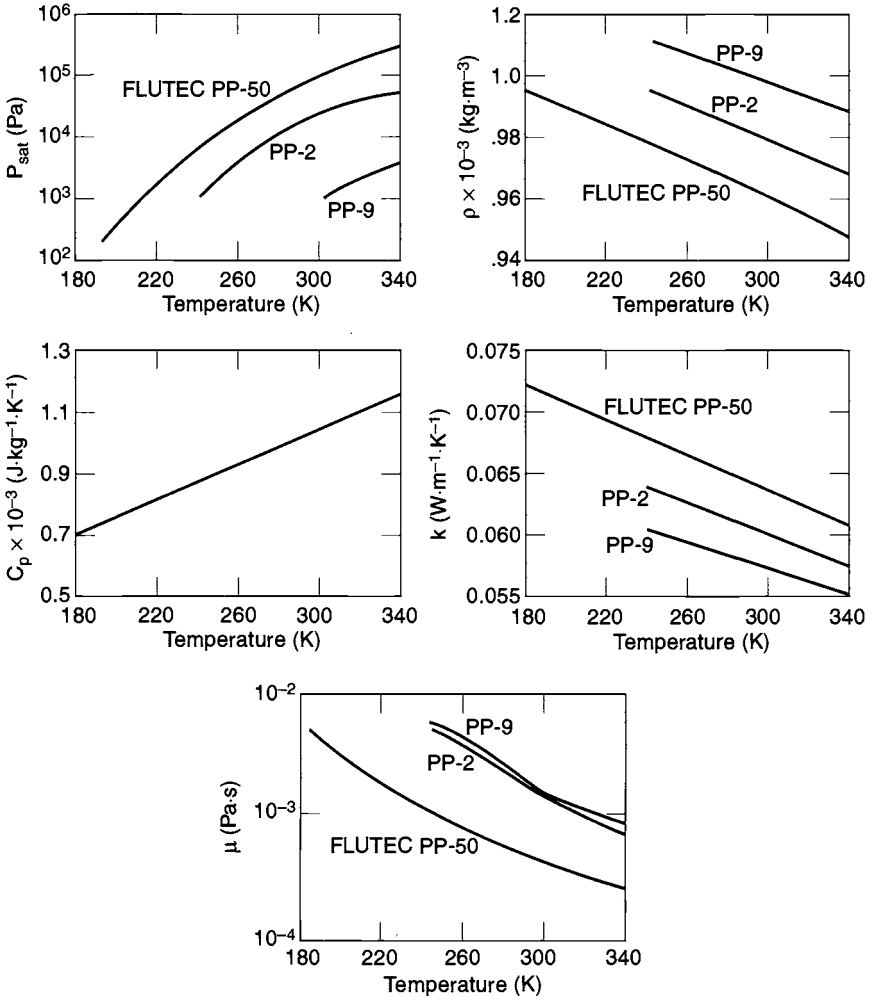


Fig. 12.18. Physical properties of Flutec PP-2, PP-9, PP-50.

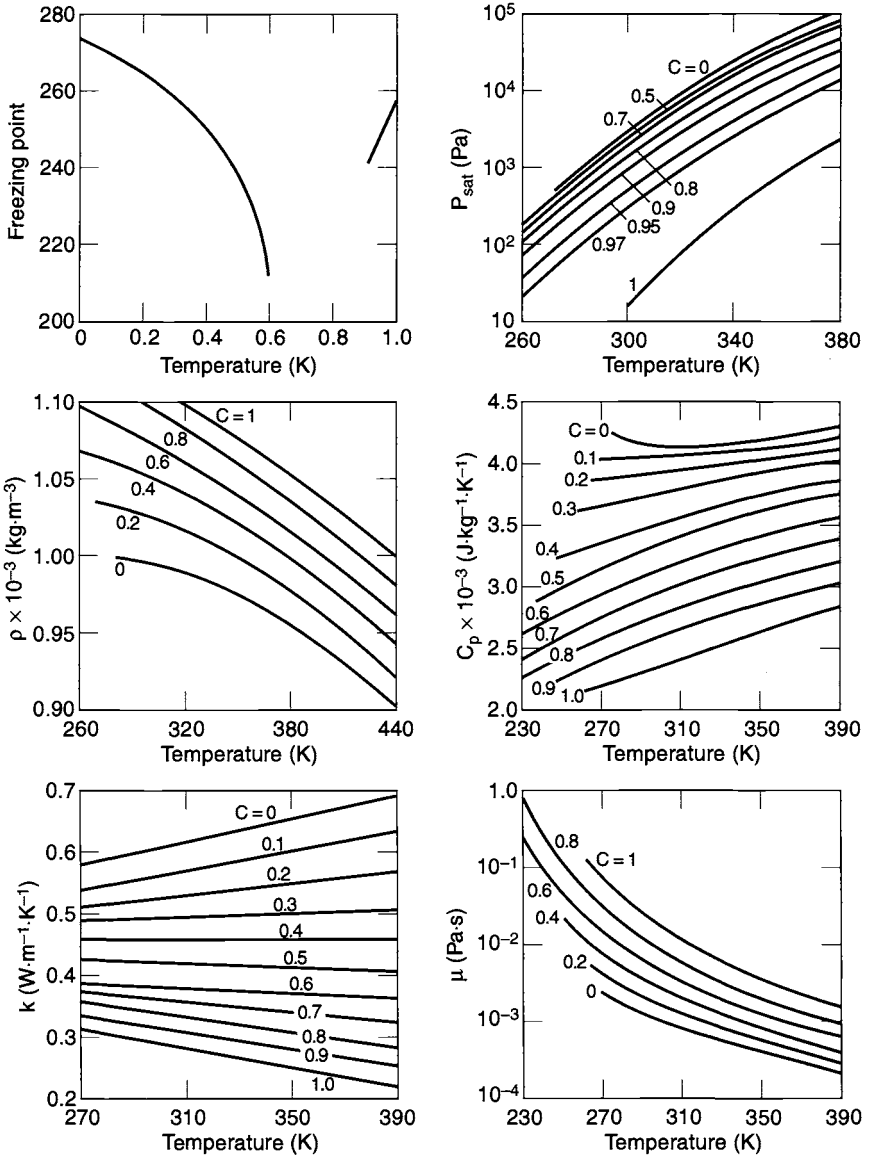


Fig. 12.19. Physical properties of water/glycol solutions.

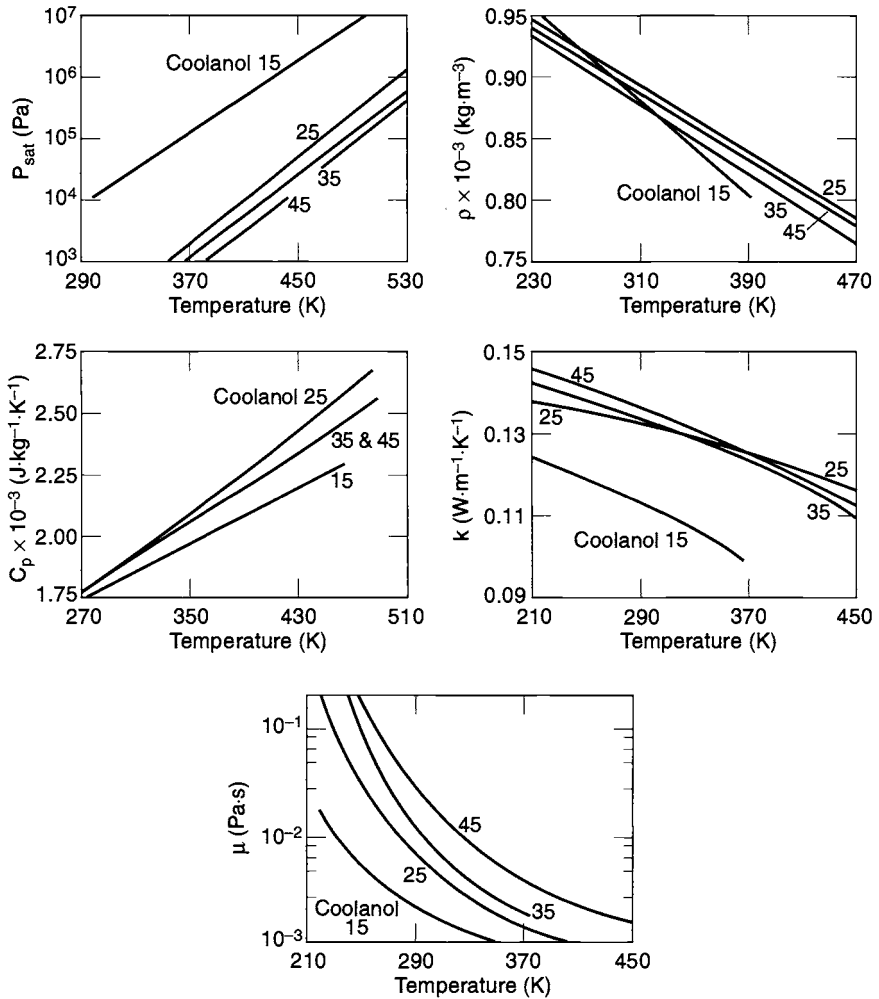


Fig. 12.20. Physical properties of Coolanol 15, 25, 35, 45.

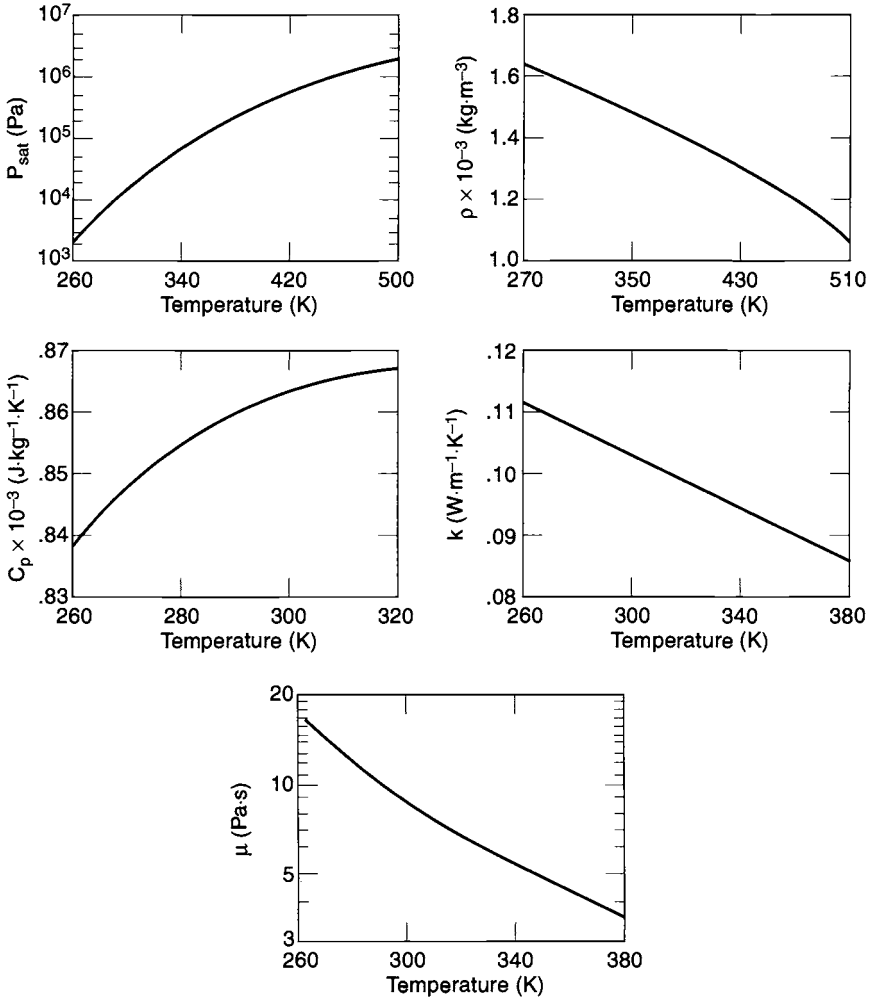
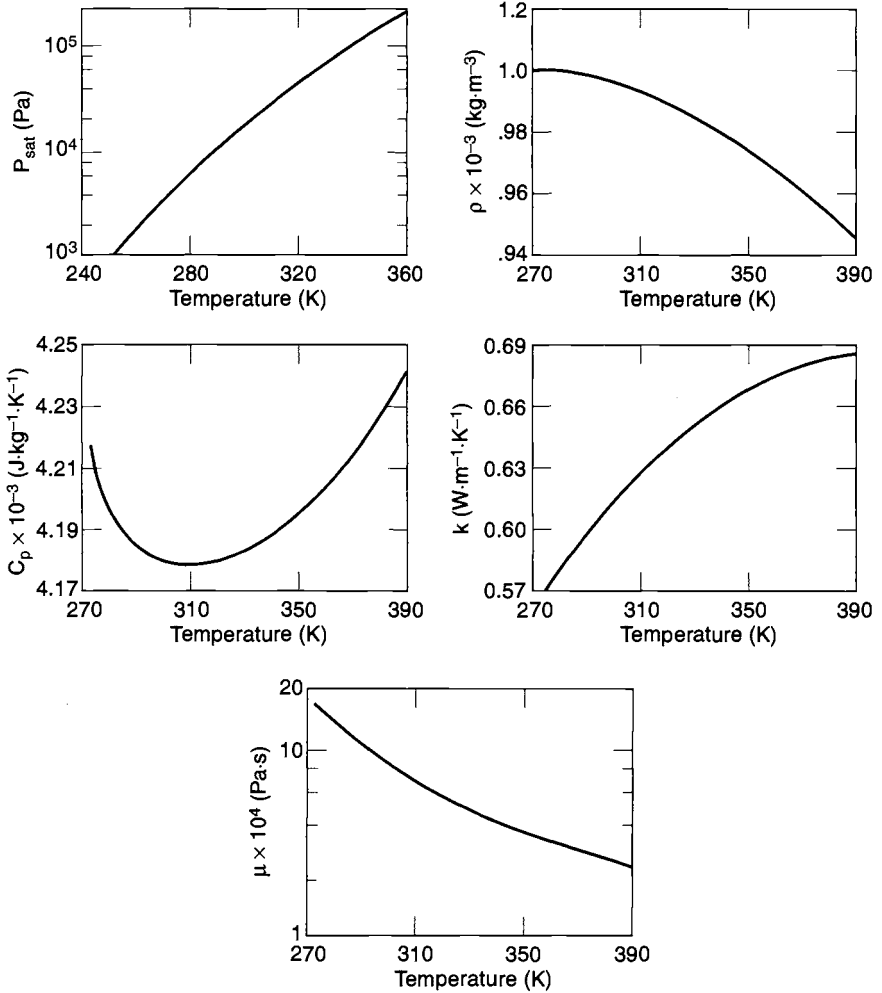


Fig. 12.21. Physical properties of carbon tetrachloride.

**Fig. 12.22. Physical properties of water.**

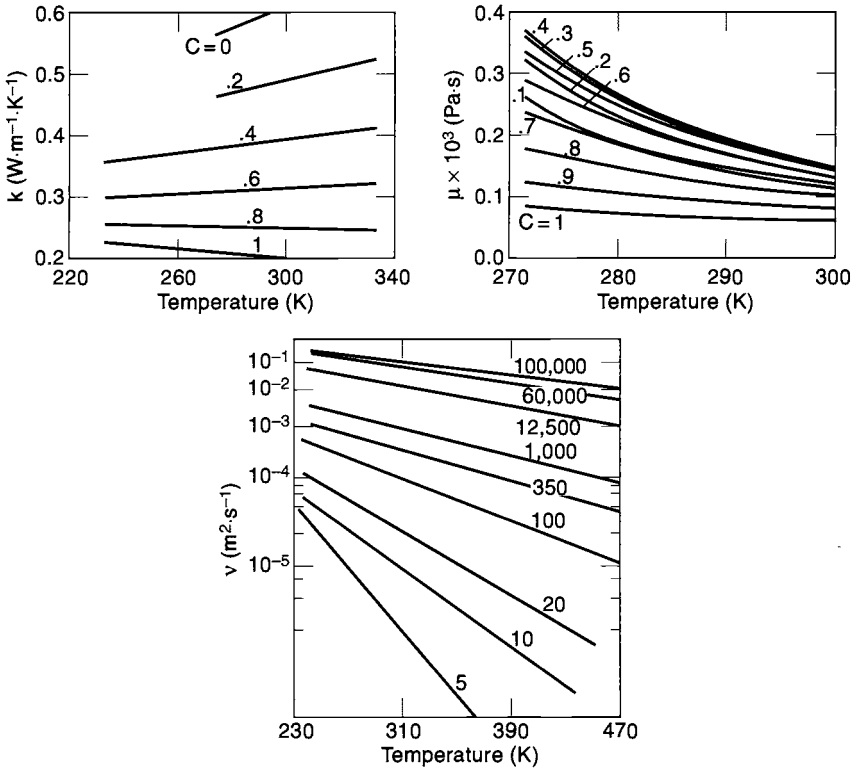


Fig. 12.23. Physical properties of methanol/water solution, DC-200.

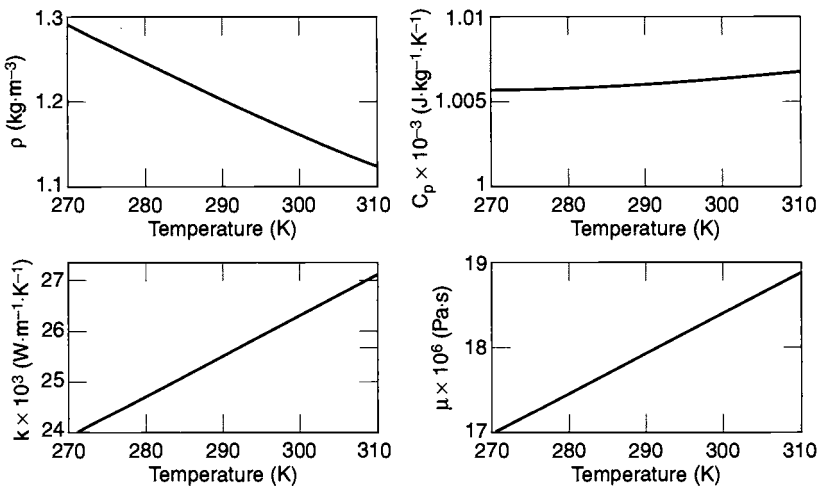


Fig. 12.24. Physical properties of air.

Analysis of a Fluid Loop

The engineering background presented in the previous sections is adequate for analyzing the fluid loop in Fig. 12.1. The design procedure in this section follows closely the analysis provided in Ref. 12.60. The following engineering data are assumed to be known for the system.

- general layout of the fluid loop, including system geometry and dimensions
- thermal properties of the coolant (k , c_p , ρ , μ)
- total heat-flow rate to be removed, Q
- mass flow rates in each loop and heat exchanger (m_h , m_c)
- inlet temperature of the cold fluid in the heat exchanger (T_{ci})

The temperatures throughout the loop and the pumping-power requirements can be determined by performing an energy balance on the system. To compute the temperatures in the loop, the heat-exchanger effectiveness must be calculated. The following steps are needed.

1. Compute the required heat-exchanger heat-transfer surface areas.
2. Compute fluid properties such as density (ρ), specific heat (c_p), thermal conductivity (k), dynamic viscosity (μ), and Prandtl number (Pr).
3. Compute the Reynolds number (Re) for each section of the loop.
4. Compute the Nusselt number (Nu) and the convective heat-transfer coefficient (h).
5. Compute the temperature effectiveness (η) of all the extended surfaces.
6. Compute the overall heat-exchanger thermal conductance (U).
7. Compute the number of heat-transfer units (NTU).
8. Compute the heat-exchanger effectiveness (ϵ).

Once all of the above engineering data are available, the temperatures throughout the loop can be calculated from these equations:

$$T_{co} = T_{ci} + \frac{Q}{C_c}, \quad (12.42)$$

$$T_{hi} = T_{ci} + \frac{Q}{\epsilon C_1}, \quad (12.43)$$

and

$$T_{ho} = T_{ci} + Q \left(\frac{1}{\epsilon C_1} - \frac{1}{C_h} \right), \quad (12.44)$$

where C_1 is the smallest of C_h and C_c .

The pumping power, P_p , required to operate the fluid system against the pressure drop, ΔP , can be calculated from the relation

$$P_p = \Delta P \frac{\dot{m}}{\rho} \cdot \frac{1}{\eta_p}, \quad (12.45)$$

where η_p is the overall pump efficiency, ΔP is the pressure loss through the system, \dot{m} is the fluid-mass flow rate, and ρ is the fluid density at the location of the pump. Thus, the term \dot{m}/ρ represents the fluid-volume flow rate through the pump. The following procedure can be used as a general guideline to compute the pressure losses within the system:

1. Compute the Reynolds number (Re) in all flow conduits.
2. Compute the friction factor (f) for the straight parts of the tubes.
3. Compute pressure loss resulting from friction along the tube walls.
4. Compute pressure loss for all pipe bends.
5. Compute pressure loss in all the fittings (e.g., valves, manifolds, entrances).
6. Compute pressure loss in heat source and heat sink.

Computer Software for System Analysis

Two of the more commonly used thermal fluid network analyzers, SINDA (Systems Improved Numerical Differencing Analyzer)/FLUINT and ESATAN-FHTS (European Space Agency Thermal Analysis Network-Fluid Heat Transfer System), are presented in this section along with a description of The Aerospace Corporation's version of SINDA. This discussion is not intended to cover all available codes, but to provide a brief overview of representative code capabilities. The interested reader should consult the reference list^{12.61,12.62} for more detail.

SINDA/FLUINT^{12.63}

Under a NASA contract, Martin Marietta Corporation undertook the task of developing an advanced SINDA thermal analysis computer program in 1983.^{12.64} The final product of the contract was SINDA '85. This version of SINDA has been improved by a series of enhancements that include the fluid-flow network capability known as the fluid integrator (FLUINT). The combined new computer code SINDA/FLUINT has both thermal and fluid network capabilities. It can perform the pressure/flow analysis of a system containing an arbitrary tube network simultaneously with the thermal analysis of the entire system being cooled, permitting the mutual influences of thermal and fluid problems to be included in the analysis. Companion codes Thermal Desktop and FloCAD provide a graphical user interface for building one-dimensional flow models within a 3-D thermal model.

FLUINT is intended to provide a general analysis framework for internal one-dimensional fluid systems. The computer code can be applied to any arbitrary fluid system; it is not restricted to specific geometries or configurations. Users can select from 20 refrigerants that are immediately available as working fluids, or they can specify their own fluid properties for any specific applications. The code can handle both single- and two-phase flow as well as transitions between these states. FLUINT also includes some common fluid-system components (pumps, valves, and ducts). Inputs are parameterized within spreadsheet-like variables, allowing complex models to be rapidly manipulated, and routines are available for automated model correlation to test data.

ESATAN-FHTS^{12.65}

FHTS was developed by GEC Engineering Research Centre in the United Kingdom as an extension of the European Space Agency's principal thermal analysis package, ESATAN. The FHTS computer code can solve both steady-state and transient fluid-flow problems. It can obtain thermal hydraulic solutions to single- or two-phase fluid-flow systems. With it, users are able to construct PFLs from basic node and conductance data to simulate hardware such as pumps and heat exchangers. By defining fluid nodes, fluid conductances, and mass flow links within the framework of ESATAN, one can perform engineering simulations for all-fluid, all-thermal, or combined fluid and thermal systems simultaneously. A variety of predefined models commonly used in fluid systems, known as fluid elements (e.g., pumps, heat exchangers, tee fittings, valves), have been included within the software to reduce the users' input effort. The FHTS has an internal library of fluid-property correlations that can simulate various types of coolant. These include water, ammonia, R11, R12, R22, R114, R502, and air. The user can specify any of these fluids by assigning the appropriate one to the nodal entity. The final system solution gives pressure and temperature (or enthalpy) at each fluid node, and mass flow rate on each fluid link. Reference 12.65 contains more detail on the FHTS.

The Aerospace Corporation's SINDA^{12.66}

A flow-network solution scheme has been implemented in The Aerospace Corporation's version of the SINDA thermal analyzer. The computer code can be used for standalone fluid flow and coupled heat-transfer/fluid-flow networks. For standalone flow problems, the flow-network solution capability can be used as a design tool to size the various flow elements such as the pipes, valves, and pump. In coupled thermal/fluid problems the coupling arises from the temperature dependence of the fluid properties. The fluid is assumed to be single-phase, viscous, and incompressible. In addition, the flow is one-dimensional and completely bounded by solid boundaries. Another major assumption in the flow solution is that the flow is always at quasi steady state. Hence, the transient pressure fluctuation is assumed to be negligible. However, the validity of this assumption breaks down for high-speed flows when shock waves are formed or when the flow becomes choked. The solution to a flow network includes the pressure distribution and the mass flow rate across each flow passage.

PFL Application**General**

A mechanically pumped single-phase cooling loop was successfully flown on the Mars Pathfinder (MPF) spacecraft, which safely landed on the Martian surface on July 4, 1997, after a seven-month cruise in space. One of the key technologies that enabled the mission to succeed was an active heat-rejection system (HRS) that cooled the electronics. This HRS consisted of a mechanically pumped single-phase cooling system for cooling the electronics and other spacecraft components on the MPF spacecraft. This was the first time in U.S. space history that an active

pumped-liquid cooling system was used in an uncrewed Earth-orbiting or deep-space-mission spacecraft.

The mechanically pumped loop was developed for the MPF mission because of the unique requirements and constraints posed by the mission.^{12.67,12.68} Several thermal control design concepts, employing hardware elements such as variable-conductance heat pipes, constant-conductance heat pipes, and detachable thermal/mechanical links, were evaluated before the selection of the pumped cooling loop.

A schematic of the spacecraft and a picture of the assembled spacecraft are shown in Fig. 12.25. The same communications and data-analysis electronics were used during both cruise and landed operations. This equipment was located

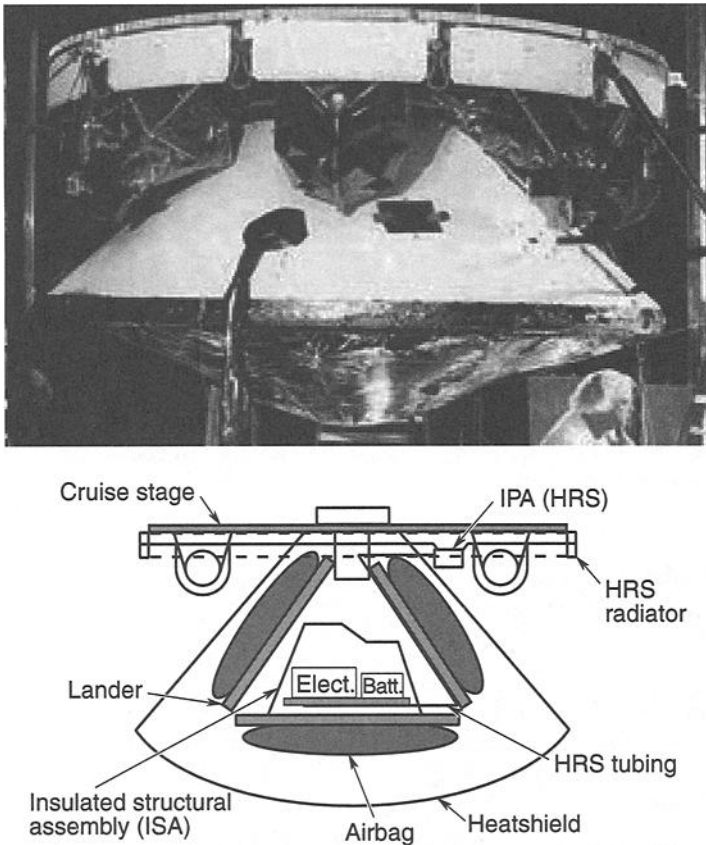


Fig. 12.25. MPF thermal control configuration. Top: MPF spacecraft completely assembled; bottom: spacecraft schematic showing the thermal control system configuration.

on the base petal of the lander and was completely enclosed in very high-performance insulation to conserve heat during the Martian nights, which can be as cold as -80°C . During cruise, the same equipment was operated continuously at about 90 W of power to communicate with ground. Passive dissipation of this heat is very difficult because of: (1) high power level, (2) high temperature outside the insulated enclosure (15°C near Earth), and (3) additional insulation from the stowed airbags. These conditions in the spacecraft configuration necessitated an HRS for Pathfinder. The main functions of the HRS were to transfer heat from the lander during cruise and minimize heat leak from the enclosure during Martian nights.

Several new approaches were used for the design, qualification, and verification of the HRS because of the short time available for its implementation on the spacecraft. The engineering and flight development were done in parallel; the whole cooling system was designed, built, tested, and installed on the spacecraft in less than two years. A description of this design, fabrication, and testing is given in Refs. 12.69, 12.70, and 12.71.

Active HRS Design

The MPF active HRS was designed to keep the key spacecraft components within the allowable temperature range. This objective was accomplished by using a mechanically pumped single-phase liquid loop to transfer excess heat from the components inside the spacecraft to an external radiator. After the mechanically pumped cooling loop was chosen to serve as the HRS for MPF, a system-level design study was performed on the spacecraft and the following requirements were developed for the HRS.

Performance Requirements

These performance requirements for the HRS were developed based on the Pathfinder mission requirements:

Physical:

1. Mass of the HRS system: < 18 kg
2. Input electrical power: < 10 W

Thermal:

1. Cooling power: 90–180 W
2. Allowable temperature range of equipment: -60 to -20°C (low limit), 5 to 70°C (high limit)
3. Freon liquid operating temperature of -20 to $+30^{\circ}\text{C}$
4. < 3 W parasitic heat loss on Martian surface (from any remnants of the cooling loop)

Integrated Pump Assembly (IPA):

1. 0.76 l/min Freon flow rate @ > 27.6 kPa pressure rise
2. < 10 W total power consumption during cruise

3. < 8 kg weight
4. > 2 years of continuous operation without failure

Leakage:

1. Meet specified (very low) leak rate (liquid and gas) to maintain liquid pressure well above saturation pressure—at least 206 kPa higher

Venting:

1. Freon to be vented from HRS prior to lander entering Martian atmosphere to prevent contamination of Martian surface (Freon would interfere with chemical experiments to be performed by Pathfinder on Mars)
2. Freon lines from lander to cruise stage to be cut by pyro cutter after Freon has been vented to allow separation of cruise stage from the lander
3. Negligible nutation torque of spacecraft resulting from venting process
4. Negligible contamination of spacecraft components during Freon venting

HRS Design Description and Trade-Offs

The HRS consisted of six distinct parts. A schematic of this system is shown in Fig. 12.26. The key components are the following:

- IPA (integrated pump assembly)
- Freon-11 working fluid (also known as Refrigerant 11)
- HRS tubing
- electronics assembly
- Freon vent system
- radiator

The primary spacecraft electronics (the key heat source) was located in the lander base petal in a highly insulated enclosure. The IPA circulated the Freon through the HRS tubing from the electronics-equipment shelf to the cruise-stage radiator. The vent system was used to vent the Freon prior to Martian entry.

IPA

The IPA had two centrifugal pumps; one was primary, whereas the second one served as backup in case the primary one failed. Only one pump was on at any time. Each pump (powered by its own motor) produced more than 27.6 kPa pressure differential at 0.76 l/min. The pump/motor assembly had hydrodynamically lubricated journal bearings to minimize bearing wear and frictional power loss, and to maximize the life of the system. Each pump/motor assembly was powered by its own individual radiation-hardened electronics.

Two wax-actuated thermal control valves automatically and continuously split the main Freon flow between the radiator and a bypass to the radiator to provide a fixed (mixed) temperature fluid to the inlet of the electronics shelf—this was to account for the continuously decreasing environmental temperature of the radiator on its journey from Earth to Mars and the constantly changing heat load on the electronics. The thermal control valves used an enclosed wax pellet with bellows to open and close two ports leading up to the radiator and its bypass depending on

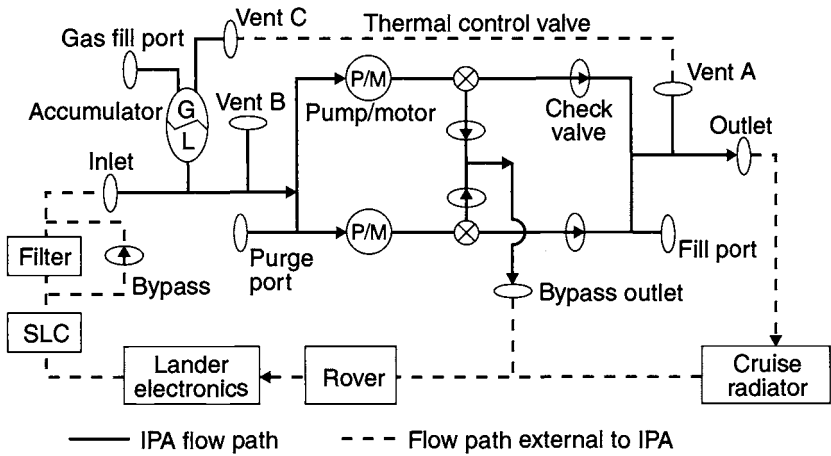


Fig. 12.26. Mars Pathfinder HRS.

the temperature of the Freon entering the valves. The set point of the valves was 0 to -7°C , a range that was chosen because it is approximately in the middle of the operating temperature limits of the electronics being cooled by the HRS. When Freon entered the thermal control valves, if the temperature was higher than 0°C , all the flow was allowed to go through the radiator, whereas when the temperature fell below -7°C , all the flow bypassed the radiator. For intermediate temperature values, the valves opened partially in each direction.

Four check valves in the IPA prevented the flow from recirculating from the primary (active) pump to the backup (inactive) pump, and they prevented bypassing of either the electronics or the radiator whenever only one pump was on and the thermal control valves were either diverting the flow fully or partially to the radiator. Because of the changing environment temperature, the bulk of the Freon liquid experienced a temperature change (-40 to $+50^{\circ}\text{C}$) during the flight and ground testing. To accommodate this, the IPA employed a bellows accumulator to maintain the liquid pressure at least $2 \times 10^5 \text{ N/m}^2$ (30 psi) above its saturation pressure throughout the flight to prevent cavitation of the centrifugal pumps. The accumulator bellows has a stroke volume of 393 cm^3 and is sized to account for a liquid volume change of 229 cm^3 because of temperature changes and liquid leaks as large as 164 cm^3 during the flight (7 months or 5100 hours). A detailed design description of the IPA is provided in Ref. 12.69.

Freon-11 Working Fluid

About 15 fluids (Ref. 12.68) were traded off as candidate working fluids before the selection of Freon-11 (CCl_3F , trichlorofluoromethane), a refrigerant commonly used for building air conditioners. The working fluid was designed to remain in the liquid phase under all conditions, to allow the mechanical pumps to work satisfactorily; this and other considerations led to the selection of several criteria used to trade off these liquids. The liquids included various Freons, methanol, ethanol, glycols, Dowtherms, and trichloroethylene. The selection criteria were:

- freezing point (should be less than about -90°C because during the radiator bypass the Freon in the radiator could get as cold as -80°C)
- boiling point (should be as high as possible to ensure that the operating pressure required to maintain the liquid state is low; also should be higher than room temperature for ease of handling during ground operations)
- specific heat and thermal conductivity (should be high); viscosity (should be low, for high heat-transfer rates and low pressure drops)
- compatibility with commonly used materials like aluminum and stainless steel (should be excellent for long-term corrosion proof performance)

The important properties of Freon-11 are:

- freezing point = -111°C
- normal boiling point = 24°C
- vapor pressure at 50°C (highest operating temperature) = 138 kPa
- specific heat = $900\text{ J/kg}\cdot\text{K}$
- thermal conductivity = $0.084\text{ W/m}\cdot\text{K}$
- viscosity = $5 \times 10^{-4}\text{ N}\cdot\text{s/m}^2$
- density = 1459 kg/m^3
- Prandtl number = 4
- very compatible with stainless steels
- very compatible with aluminum at low moisture levels ($\sim 10\text{ ppm}$)
- quite corrosive at high moisture levels ($\sim 100\text{ ppm}$)
- compatible with some elastomers, such as Viton, and materials like Teflon

Tube Diameters and Materials

Tube diameters of 12.7, 9.53, and 6.35 mm (1/2 in., 3/8 in., and 1/4 in.) were traded off for heat transfer, pressure drop, pumping power, and weight. Tubing with a 6.35-mm (1/4 in.) diameter was used for the electronics shelf for high heat transfer and the fact that the length was short enough (1 m) that the consequent pressure drop was not excessive. Tubing with a 9.53-mm (3/8 in.) diameter was used for the radiator because the heat-transfer coefficient was not critical in the radiator (large available area, about 8.22 m long); 9.53-mm (3/8 in.) tubing was also used for the transfer lines. The radiator and the transfer lines had long lengths of tubing; this also minimized the pressure drop in the loop. Freon flow rates were traded off in terms of heat transfer and pressure drops to come up with an optimum value of 0.76 l/min.

The electronics shelf and radiator used aluminum tubing because the tubing in these zones was brazed to aluminum surfaces that were used to ensure high heat-transfer rates with minimum weight. The transfer lines were made of stainless steel for ease of welding, better compatibility with Freon, shorter lengths, and lack of heat-transfer requirements.

Electronics-Shelf Tubing Layout

Several tubing layouts were investigated to minimize component temperatures, Freon pressure drop, and pumping power. The key constraints were the temperature limits of the solid-state power amplifier (SSPA; 40°C) and the battery (-20 to $+25^{\circ}\text{C}$), and the highly localized heating in the SSPA (43 W in a relatively small area). The cooling-loop tubing was strategically routed and wrapped near the

high-power-dissipation area of the SSPA to minimize its temperature rise; the other electronics boxes had a relatively uniform power dissipation and did not require strategic routing of the cooling-loop tubing to pick up their heat.

The shelf's facesheet thickness was varied to trade off heat transfer and mass. Local thickening of facesheet near hot spots was also investigated. A basic thickness of 1.5 mm for the facesheet (no local thickening) was chosen, which satisfied all the thermal requirements. After MPF's entry into the Martian atmosphere and landing, the HRS was no longer functional, and the electronics in the lander relied on its thermal mass to manage its temperatures within its limits. Since the SSPA power density was so high, the facesheet was thickened near the SSPA to 4.5 mm to satisfy the entry and Martian surface requirements (coupling the high-power, low-mass SSPA to the low-power, high-mass IEM (integrated electronic module) box to improve the transient response).

In addition to the lander electronics shelf, two other components were cooled by the cooling loop: the shunt limit controller (SLC) and the Rover cold finger. The Rover cold finger is coupled to a split clamshell, which grabs onto the HRS tubing to reject its heat (2 W). The SLC had a heat dissipation varying from 0 to 60 W (depending on the shunted power), and its cooling was achieved by bonding a cold plate to its interface—two feet of the cooling-loop tubing were brazed to the cold plate for Freon flow.

Venting

Before MPF entered the Martian environment, the Freon had to be removed from the lander (to minimize contamination of the Martian surface) by either venting all of it to space or repositioning it to the cruise stage (which was separated from the lander before entry). Several schemes to vent the Freon were investigated before engineers came up with one that minimized the resultant torque on the spacecraft. One method proposed the use of high-pressure gas (N_2) in the accumulator to "piston out" Freon from the HRS by opening a pyro valve that connects the gas side of the accumulator to the liquid; the liquid in turn would be vented to space via a nozzle that is opened to space via another pyro valve. Another method proposed discharging the Freon from opposing (T-shaped) nozzles to cancel the torques, or, through a single nozzle with the nozzle axis passing through the spacecraft center of gravity (c.g.), with the nozzle outlet pointed in a direction opposite to the c.g.

The main reason for the torque on the spacecraft is the reaction from the momentum of the venting Freon; hence the rationale for entertaining the possibility of repositioning the Freon, because until the spacecraft is intact (with the cruise stage connected to the lander), repositioning the Freon within the spacecraft should minimize the reactional torque. The proposed scheme was to use the accumulator gas to push the Freon into a separate (extra) thin-walled and lightweight "holding" tank in the cruise stage (sized to hold the entire volume of liquid Freon). An extra check valve would prevent backflow from the holding tank to the HRS.

Venting Freon to space through a single nozzle with its axis passing through the spacecraft c.g. was the venting method that was chosen and implemented, a simple scheme to implement with minimum contamination and minimum hardware changes to the spacecraft. The diameter of the nozzle was 1 mm, which met the attitude-control system's requirements for the disturbing torque—the time to vent

all the Freon was predicted to be about three minutes. The initial thrust from the nozzle was estimated to be about 0.5 N with an initial exit speed of 21 m/s. The thrust, of course, decays very rapidly (exponentially) and is less than 0.05 N at the end of the vent process.

Radiator

The radiator used to reject the 180 W of heat (maximum) is 8.22 m long by 0.2 m wide. It is a circumferential strip of aluminum (0.75 mm thick and thermally attached to the 9.53-mm-diameter HRS tubing) located at the circumference of the cruise stage. It is mechanically attached to the cruise-stage ribs and thermally (conductively) decoupled by isolators. Both sides are painted white (NS43G on the outside surface, Dexter Crown Metro gloss white on the inside surface; high α , low ϵ) to maximize the radiator's heat-loss potential. The inside surface is radiatively coupled to the warm cruise stage underside and the backshell to preclude freezing of the Freon in the radiator when the radiator faces a cold environment and most of the Freon bypasses the radiator (94% bypass).

The reason for relying on the radiative coupling instead of the conductive coupling to pick up some heat from the cruise stage is that the radiative coupling (and heat input) is much easier to predict and implement than the conductive coupling. This is the case because the conductive coupling is achieved via a very convoluted and complex thermal path that also involves contact conductances. For the coldest conditions the cruise stage is at -30°C while the backshell is at -65°C —these surfaces provide enough heat to the radiator in the coldest conditions to maintain the temperature of the coldest portion of the radiator above -80°C , which is well above the freezing point of the Freon-11 (-111°C). The radiator temperature would not fall below -80°C even if there were no Freon flow through the radiator.

IPA Design, Fabrication, and Test

The IPA, which is a major element of the HRS, circulates and controls the flow of Freon-11 in the mechanical cooling loop. It consists of mechanical centrifugal pumps, an accumulator, thermal control valves, and control electronics. The specifications, design, and implementation of the IPA in the Pathfinder HRS are described in Ref. 12.69. The key new technologies developed and implemented in the system are the use of Freon-11 as a single-phase working fluid and a wax-actuated thermal control valve to control the fluid temperature in the loop. A description of the thermal control valve is given in Ref. 12.69.

IPA Specifications

The IPA design specifications were based not only on the spacecraft thermal control considerations but also on the spacecraft system-level considerations of reliability, mass, power, and cost. As a consequence, the overall system consisted of redundant pump systems: each unit had its own pump/motor, motor-control electronics, check valves, and thermal control valve to bypass the flow. The only non-redundant component in the IPA was the accumulator. The specified arrangement of the components in the IPA is shown in Fig. 12.26.

The specifications developed for the IPA covered hydraulic and electrical performance, component descriptions, mechanical and electrical design, electronic

and mechanical parts, electromagnetic compatibility, operating and nonoperating environments, fabrication and assembly requirements, and quality-assurance provisions. The key specifications are listed in Table 12.12.

Design and Fabrication

The detailed mechanical and electrical design of the IPA was developed by the vendor based on the specification provided by JPL. The mechanical design consisted of four major components mounted on a baseplate: the accumulator, the

Table 12.12. Key IPA Specifications

Section	Specification Detail
Thermal and hydraulic	
Flow rate and pressure rise	Freon flow rate of 0.76 l/min, at 27.6 kPa in the operating temperature range of -20 to 30°C
Maximum operating pressure	690 kPa
Operating temperature range	-30°C to 40°C
Bypass ratio	Above 0°C, 100% radiator flow; below -7°C, 100% bypass flow
Leak rate	Helium leak rate of 10^{-7} scc/sec for the gas and 10^{-4} scc/sec for the liquid side
Storage temperature	-40°C to 50°C
Physical	
Mass	Maximum of 8 kg dry
Size	25.4 × 25.4 × 16.5 cm
Service valves	One for gas charge and two for liquid fill and purge
Mounting	Mounted on a base plate
Operation	
Life	10,000 hours continuous, 3 calendar years
Starts/stops	1000
Electrical	
Input voltage	To operate in 27 Vdc to 36 Vdc
Power	10.6 W maximum
Isolation	One MΩ electrical isolation
Electronics parts	MIL-STD-975 Grade 2; MIL-STD-883C Grade B for microcircuits; withstand a radiation environment of 500 rads (SI); CMOS and MOSFETs meet single-event effect parameters
Acceptance tests	IPA hydraulic performance, sinusoidal and random vibration, thermal vacuum test, proof pressure, and leak-rate tests

pump/thermal control manifold, an electronics box housing all the motor-control electronics, and a front panel housing the service valves. The materials used for the IPA were 304L stainless steel, Inconel 718, and aluminum. Stainless steel was used for all the wetted paths of the IPA except the accumulator bellows, for which Inconel 718 was used, whereas aluminum was used for the baseplate and the electronics box. The electronics box was designed as a modular unit so that it could be removed from the pump assembly during welding of the pump assembly to tubing that would circulate Freon in the spacecraft.

The accumulator featured a welded Inconel 718 double-walled bellows to contain the Freon liquid with the pressurant gas (nitrogen) on the outside of the bellows. The stroke volume of the bellows was 393 cm³. A service valve was mounted on the housing to provide access to charge the accumulator with gas to the required pressure. A strain-gauge-type pressure transducer was welded to the accumulator housing to measure the gas pressure during ground operations and testing. The pump manifold was machined from wrought stainless steel, which housed the check valves, thermal control valves, pump/motors, and the inlet and exit ports.

A centrifugal pump was chosen over other types of pumps on the basis of life and reliability data on pumps and the suitability for the current application. The hydraulic performance and electrical-power requirements of the Pathfinder HRS favored the centrifugal-type pump. The Pathfinder HRS required a small pressure rise at a large flow rate, and it had very little power available for the pumps. At the required performance point of 0.76 l/min at 27.6 kPa, the specific speed of 1267 predicted a pump head efficiency of 10% for a centrifugal pump, meeting power requirements. The concept of using a positive-displacement pump was rejected because of a lower service life and material restrictions. The selected pump featured a radial vane Barsky-type impeller, driven by a brushless DC motor with Hall effects sensors embedded in the stator. The impeller was a four-vane design without side shrouds to minimize viscous losses, and it was attached directly to the motor shaft. The motor rotor, which rotates at about 12,000 rpm, was supported by two carbon graphite journal bearings, lubricated by the working fluid. The rotor consisted of permanent magnet poles made of Samarium Cobalt. A stainless-steel sleeve isolated both the rotor and stator from the working fluid. This wet design negated the need for a shaft seal, improving the pump life.

The vendor had used this design a few years earlier for a developmental unit for another program. This unit was ground-tested and had run for about 3000 hours and experienced more than 300,000 starts and stops. The clearances in the pump varied from about 6 μm in the journal bearings to 125 μm in the bypass loop for wetting the journals. Two developmental pumps were first built for the Pathfinder program as life test unit pumps. These pumps went through thermal cycles and random vibration tests, and one of the units, shown in Fig. 12.27, was life tested. This pump had operated for more than 14,000 hours as of August 1997. Details of these tests are given in Ref. 12.71.

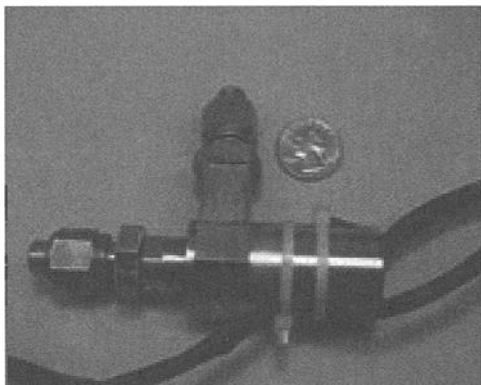


Fig. 12.27. Engineering model of the centrifugal pump used in the IPA life tests at JPL.

The check valves used were made of stainless steel with a cracking pressure of 1.4 kPa. These valves used Teflon O-rings as seals. The thermal control valve used a wax actuator that provided an actuation of 0.5 mm within a temperature range of -7 to 0°C . The actuator moved a spool in the valve that opened or closed the bypass port depending on the temperature of the Freon flowing through the valve. The wax was hermetically sealed from the working fluid by a stainless-steel bellows, preventing wax loss through a dynamic seal, as is common to most wax actuator designs. The original design consisted of stacked bimetallic discs. However, some developmental tests revealed that the disc material was not compatible with Freon and that the discs did not produce smooth linear motion because of stiction. Therefore, a new development effort was undertaken to build a wax actuator that would meet the Pathfinder needs.

The motor-control electronics was enclosed in a wrought-aluminum box housing the circuit-card assemblies of both the pump/motors. A connector was mounted on one end of the box for the input power, and another connector on the bottom box connected the motor controller to the pump/motors. The circuit cards were multilayer boards with lead-in components soldered to the boards. The circuits were designed to meet the Pathfinder fault-tolerance requirements for radiation susceptibility. The parts used met the reliability requirements (MIL-STD-975 Grade 2 and MIL-STD-883C Grade B). The single-event effect-sensitive parts used were JPL-approved radiation-hardened parts. EMI filters were included to meet the conducted and radiated emissions and susceptibility requirements of the Pathfinder spacecraft.

The fabrication was done in three major subassemblies before the whole unit was put together: the accumulator assembly, the pump manifold assembly, and the motor-controller electronics subassembly. The accumulator and the pump manifold were all welded stainless-steel units, whereas the controller electronics housing was in a hogged-out aluminum box with a bolted-on lid. The welds were made to qualify weld schedules by MIL-STD-1595 certified weld operators. The sample welds were made on the day of the flight weld and inspected under high magnification for sound weld quality (depth of penetration, porosity, cracks, etc.) before

the actual hardware was welded. The unit was leak-tested before the next series of welds was undertaken.

The accumulator assembly consisted of the machined housing, the bellows, service valve, pressure transducer, and purge tubing. All the parts were cleaned thoroughly to remove the particulates above 25 μm in size before the parts were assembled, tested, and welded. The unit was tested for leak rate and bellows performance between each series of welds. Electron-beam welds were used for all the welds in the accumulator subassembly. After the assembly was completed, the pressure transducer output was calibrated against pressure-gauge readings.

All the motor assemblies, valves, and inlet and outlet tubing were assembled into the wrought-stainless-steel pump manifold. All these parts were welded into the block using laser welding. Because of the magnetic properties of the motors, electron-beam welds could not be used for this assembly. As in the case of the accumulator fabrication, the pump manifold parts were cleaned and the unit tested between each series of welds. The tests consisted of checking the performance of each pump and thermal control valve, and the check valves, before the next series of welds was made.

The motor controller was designed using discrete electronic components. Two reasons led to the selection of this option rather than an integrated-circuit-based design. The first was the tight schedule for the design and fabrication of the controller. The second reason was the flexibility the discrete-component design allowed in the use of the available electronic parts. The motor-controller electronics-box fabrication consisted of fabricating the circuit cards and populating them with parts. The multilayer circuit cards were fabricated to MIL-P-55110. All the lead-in components were soldered to the boards per the MIL-STD-2000. The boards were conformally coated before they were installed in the box.

The final dry mass of the IPA before it was installed on the spacecraft was 8.3 kg. The IPA in its final assembled state is shown in Fig. 12.28.

Performance Tests

Three types of performance tests were done on the IPA: hydraulic, electrical, and system proof-pressure and leak. The hydraulic performance tests were conducted to verify that IPA met the specification requirements. These requirements related to the flow rate and pressure rise at various temperatures. The IPA flow rate at various pressure rises is shown in Fig. 12.29 for the IPA with one pump operating.

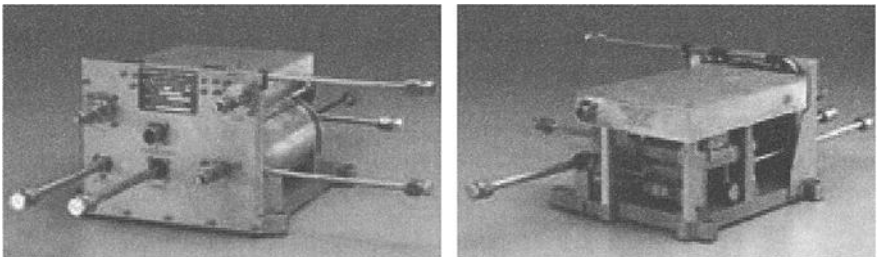


Fig. 12.28. Pathfinder IPA.

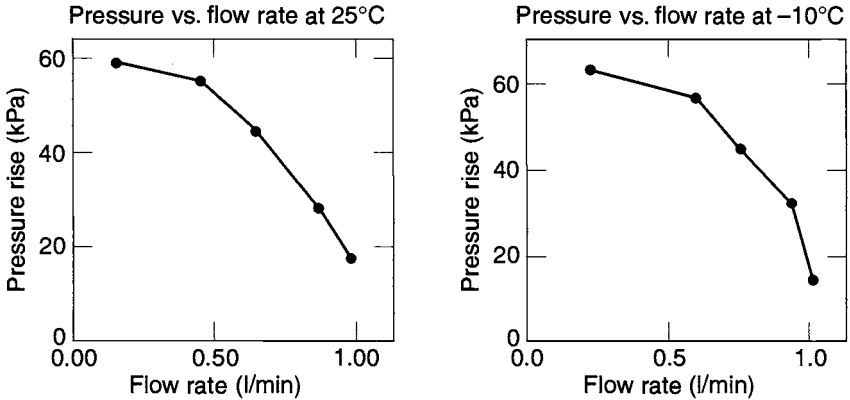


Fig. 12.29. Pressure rise vs. flow rate performance tests on IPA.

In the electrical performance tests, the current draw of the IPA at various flow rates was measured. The input voltage to the IPA was varied between 27 Vdc and 36 Vdc, and the IPA current draw was measured. The IPA electrical performance is shown in Fig. 12.30.

To verify the integrity of the IPA fabrication, the unit was proof tested and leak checked. The unit was successfully tested to a proof pressure of 1275 kPa. Two leak rates were specified for the IPA—one for the gas side of the accumulator and a second for the rest of the unit, which is the liquid side. For the gas side, the maximum leak rate was specified at 2×10^{-7} scc/sec of helium, whereas for the liquid side, it was specified as 1×10^{-4} scc/sec helium. The leak rates for each weld and valve were computed based on these total leak rates and were tested to the computed levels during the leak check of the assembly.

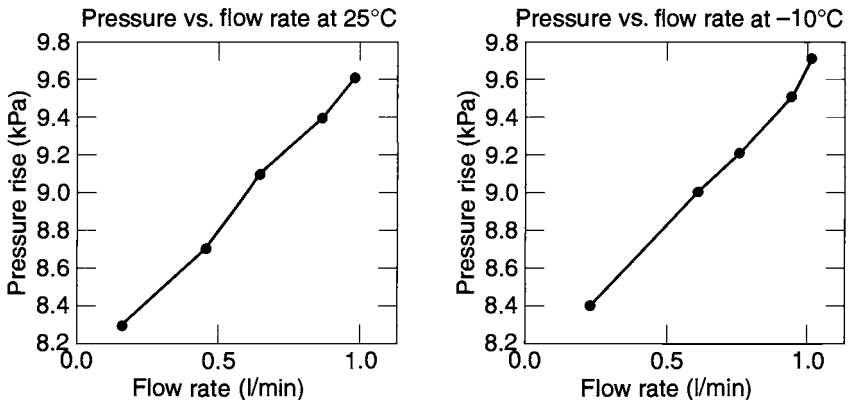


Fig. 12.30. Power vs. flow rate performance tests on IPA.

Qualification Tests

Three types of qualification tests were done on the IPA besides the performance tests: vibration tests, thermal vacuum tests, and electromagnetic compatibility and susceptibility tests. The unit was tested to protoflight levels because the flight unit was used instead of an engineering model to flight-qualify the IPA. The order of the acceptance tests is given in Table 12.13.

The test requirements for the sine and random vibration tests are given in Table 12.14. The IPA successfully underwent these tests while both the pumps were operating. The performance was monitored during the actual vibration. The sine vibration test consisted of sweeping at the specified sinusoidal amplitude levels from the lowest frequency to the highest frequency and back to the lowest frequency at a rate of 2 octaves/minute in each of the three orthogonal axes. The random vibration tests were conducted for one minute per axis. Accelerometers were used to monitor the responses during both the tests.

The thermal vacuum test on the IPA consisted of two types of tests. The first was done on the motor-controller electronics separately. The electronics box was mounted on a baseplate that was maintained at 70°C while both pumps were continuously on for a seven-day period. Electrically simulated loads were used for the pumps in this test. The second thermal vacuum test was conducted on the whole IPA and consisted of a one-day cold and two-day hot soak.

Table 12.13. IPA Acceptance Tests

Type of Test	Verification Purpose
Performance	Performance of the IPA before the start of the qualification tests
Sine vibration	Design for the protoflight launch loads
Random vibration	Design for the protoflight launch loads
Functional	Functionality of the unit after acceptance test
thermal vacuum	Design for the protoflight temperature range
Functional	Functionality of the unit after acceptance test
Proof pressure	Design for the operating pressure
Leak-detection	Leak rates of the IPA
Performance	Performance of the IPA at the completion of qualification tests

Table 12.14. Sine and Random Vibration Specifications for IPA

Axis	Protoflight Test Level	Frequency Band
Sine vibration—All	1.27 cm double amplitude 10.0 g (acceleration 0-to-peak)	5–20 Hz
Random vibration—All	+ 6dB/octave	20–80 Hz
	0.2g ² /Hz	80–700 Hz
	–12 dB/octave	700–2000 Hz
	13.2 g _{rms}	Overall

The flight cooling system was tested at two levels, the assembly level and the spacecraft level. At the assembly level, tests were done to verify the performance of the subassemblies, such as the IPA. Here the hydraulic, electrical, and thermal performance of the IPA was tested. In addition, the IPA was subjected to the thermal vacuum, random and sinusoidal vibration, and electromagnetic interference and compatibility (EMI and EMC) tests to qualify it for the flight.

The EMI qualification tests for conducted emissions and susceptibility were done on a separate life test pump/motor unit that was of the same design as the flight pump/motor unit and the flight electronics. The EMI tests were performed for the power-line ripple and power-line transients for both emissions and susceptibility. The EMI qualification tests for radiated emissions and susceptibility were performed at the spacecraft level. The IPA went through the tests and satisfactorily met the spacecraft requirements.

The IPA was bolted and welded onto a support structure before being installed on the spacecraft. Apart from the IPA, the support structure housed the HRS filter, pyro/vent system, and a heat exchanger for the shunt electronics box. Two views of the support structure are shown in Fig. 12.31. Figure 12.32 shows the IPA installed on the cruise stage of the assembled spacecraft.

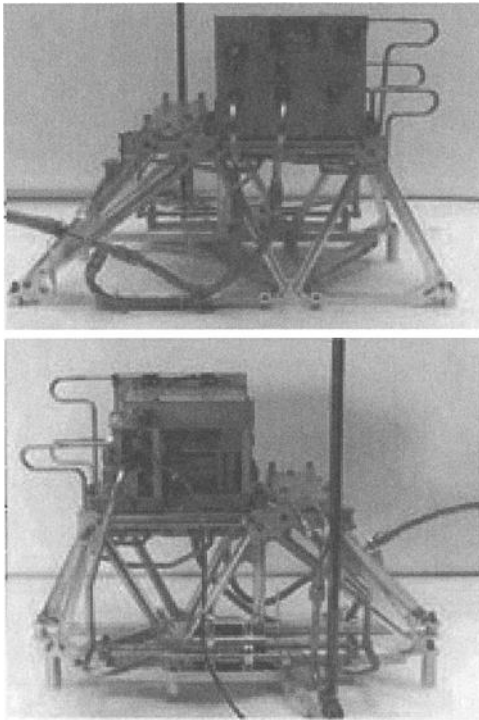


Fig. 12.31. Support structure with the IPA installed.

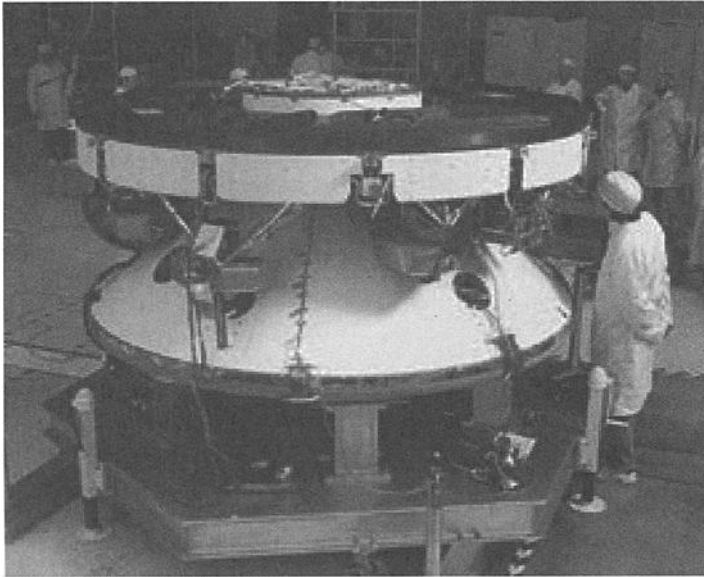


Fig. 12.32. Assembled spacecraft with the IPA installed on the cruise stage.

At the spacecraft system level, the whole system went through a series of system-level tests. These tests consisted of vibration, EMI and EMC, and system thermal vacuum tests. The end-to-end performance of the HRS was tested during the thermal vacuum test.

HRS Development Tests

Several development tests were conducted to characterize the performance of the cooling loop. These tests, performed in parallel with the design effort, were very helpful in ensuring that the final design would meet its requirements.

Thermal and Hydraulic

A development test was performed to simulate the electronics shelf and the radiator to validate the thermal and hydraulic performance models used in predicting the performance of the cooling loop. Details of these tests are given in Ref. 12.68.

Leaks

Because of integration constraints, 17 mechanical joints (B-nuts or AN fittings) were used to complete the assembly; the rest of the assembly is welded. Any large leaks from the HRS during the seven-month flight to Mars would seriously jeopardize the mission. Welded joints were not deemed to leak any significant amount of Freon. The B-nuts, however, being mechanical in nature, could potentially leak, so conducting tests on them was considered highly desirable, to ascertain that they would not leak at rates substantial enough to deplete the flight accumulator during the mission. Also desired were better schemes for providing extra insurance against potential leaks (such as epoxying the joints).

An extensive test was conducted for assessing the Freon leak rate through the mechanical joints (B-nuts or AN fittings) in the MPF HRS. All the combinations of materials (aluminum, stainless steel) and sizes (1/4 in., 3/8 in.) used in the flight HRS were simulated. Teflon flex lines identical to the flight ones were also tested for leaks through their joints. Use of epoxies to provide insurance against leaks was also assessed. Twenty-four B-nut joints were examined; they were subjected to cyclic mechanical flexing and torsion to simulate the experiences encountered by the worst joint in the flight system during launch. This testing was followed by thermal cycling to simulate the excursions during ground testing and flight.

Helium leak tests were conducted on each joint under vacuum and under internal pressure of 690 kPa. In addition, all the joints were pressurized with liquid Freon-11 (used in flight system) and tested for Freon leaks. All the tested joints exhibited leak rates that were much lower than those used to size the flight accumulator—it was sized to accommodate a leak of 164 cm³ of liquid Freon in the seven-month flight, whereas tests showed that the total leak should be much less than half of this value even under the worst conditions. Use of soft cone seals and retorquing was recommended, as well as the use of an epoxy on the exterior surfaces of the joints' leak paths.

Material Compatibility

Within the HRS, Freon-11 was in constant contact with materials like aluminum, stainless steel, and some elastomers. Concerns for potential corrosion of aluminum, particularly in contact with moist Freon, were alleviated by conducting tests to investigate the compatibility of Freon-11 with aluminum and stainless steel. Several test samples of aluminum and stainless steel were inserted in Freon-11 with different levels of moisture. (Freon is supplied in drums at a moisture level of about 10 parts per million, and it saturates at 100 ppm.) These samples were examined chemically, visually, and under electron microscopes to measure the levels of corrosion as a function of time. For aluminum, no evidence of corrosion was observed for low moisture levels (close to 10 ppm) but a very strong evidence of corrosion was observed at the high moisture levels (those much higher than 10 ppm and close to 100 ppm). This test showed the extreme importance of minimizing moisture to prevent corrosion of aluminum, and elaborate safeguards were taken in the Freon storage and loading process to minimize the moisture levels (to levels not much more than the 10-ppm level, as in the manufacturer-supplied Freon drums).

No evidence of corrosion was observed for stainless steel for all the moisture levels tested. Viton (used in the check valves) was found to swell significantly when inserted in Freon-11; however, subsequent leak tests performed on the check valves demonstrated that the leaks through them in the check direction were very small and well within acceptable limits. All other materials in contact with the Freon underwent long-term compatibility tests and were found acceptable.

Performance of the Pumped Loop during Life Tests

A life test cooling loop was built and subjected to long-term operation to verify the reliability of the various components of the flight HRS. A schematic of the setup is shown in Fig. 12.33. The life test simulated the long-term operation of the

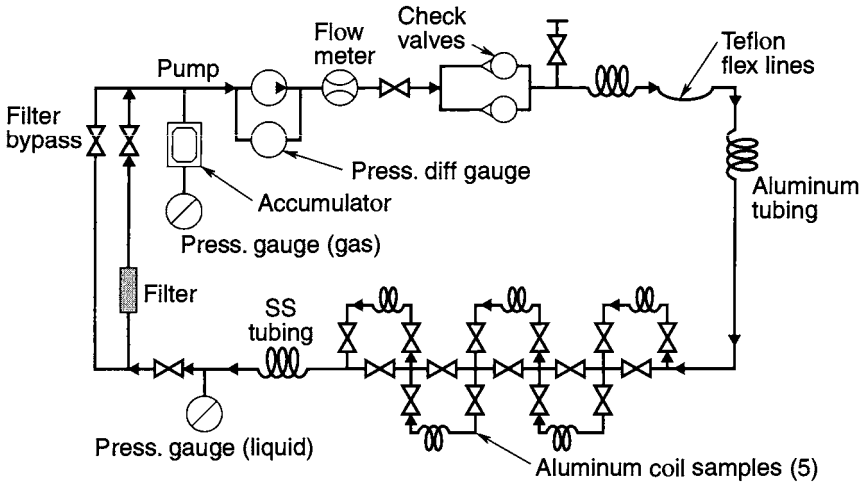


Fig. 12.33. MPF HRS life test schematic.

pump assembly, particle filter, and the rest of the HRS (aluminum and stainless-steel tubes, Teflon tubing, accumulator, check valves, etc.). A detailed description of this setup is given in Ref. 12.69.

The life test was also used to investigate and measure the long-term corrosion of the HRS tubing materials (aluminum and stainless steel) in a flowing environment with all the materials and components used in the flight system. Samples of tubing and the working fluid were taken out and tested periodically. Further, the long-term leak rates of the HRS were monitored during the life test.

Life Test Cooling Loop

Because the cooling loop was used throughout the flight for seven months (5100 hours), and its reliable functioning throughout this duration was critical to guarantee mission success, a life test setup was built and is undergoing long-term testing. The schematic of this test is shown in Fig. 12.33. It simulated the long-term operation (> 5100 hours flight duration) of pump assembly and particle filter, in conjunction with the rest of the HRS (aluminum, stainless steel, Teflon tubing, accumulator, check valves, etc.). This system clocked about 18 months (14,000 hours) of uninterrupted operation with no pump failures, exceeding the 5100 hours required for flight by more than a factor of two.

In addition to the compatibility tests described earlier (performed on small sections of tubing materials in a nonflowing environment of Freon), this life test was also used to investigate and measure the long-term synergistic corrosion of the HRS tubing (aluminum, stainless steel) in a flowing environment with simulation of all the materials and components used in the flight system. Samples of aluminum tubing and Freon liquid were taken out periodically for analysis; no evidence of corrosion was found in the first seven months. The sampling was not followed up after this period because of the severe budgetary constraints.

This life test was also used to measure long-term leaks from the HRS, particularly those resulting from mechanical joints (AN fittings, B-nuts). Relatively large leaks were observed in the beginning of the test, and they were corrected. They prompted a more elaborate leak test that was conducted separately (this test was discussed earlier).

Fig. 12.34 shows the variation in the flow rate, pressure drop, and pump input power as a function of time for this life test. During the first five months of the test the filter was slowly getting clogged (at the end of this period the filter got so clogged that it was bypassed; this situation is discussed below), the flow rate dropped to about half its value at the start of the test, the pressure drop across the system increased by 20%, and the pump input power decreased slightly.

As soon as the filter was bypassed, the flow rate increased to a value even larger than at the beginning of the test (25% larger because of the lack of the pressure drop associated with even a virgin filter); the pressure drop in the system was lower than at the beginning of the test by 15%, and the power level was about the same. These changes make sense, because the bypassing of the clogged filter reduced the overall resistance of the loop and allowed a greater flow rate at smaller pressure differences. Since even a virgin filter has a nonzero resistance, the flow rate without the filter was even larger than it was at the beginning of the test, when an unclogged filter was in the flowing loop.

The flow rate and the pressure drop across the system remained essentially constant after the filter bypass; however, the power level did fluctuate as a result of leaving the pump idle because of inadvertent power outages. A more detailed description of these effects is presented next.

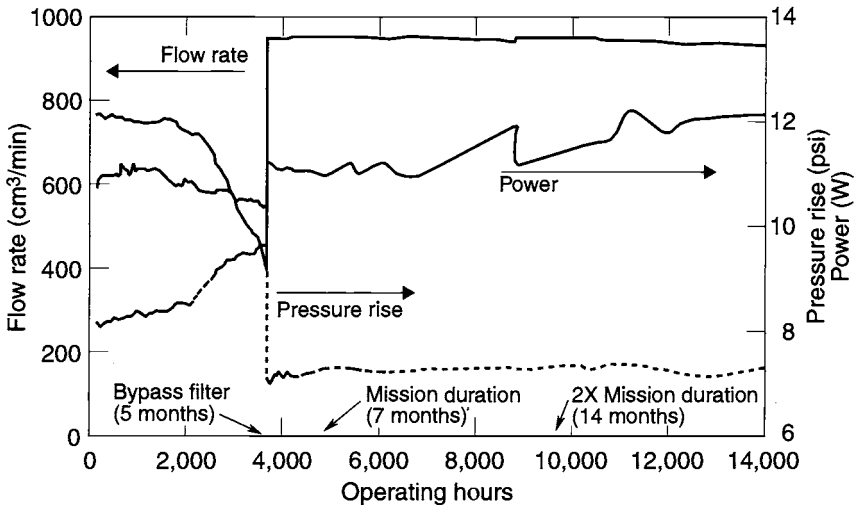


Fig. 12.34. Life test performance.

Filter Clogging

The filter used in this mock-up had inadequate capacity and was bypassed after 3600 hours or 5 months. (The flight filter had a capacity for particles at least six times higher.) To avoid the potential for significantly reduced flow rate resulting from a clogged filter, the flight filter used a check valve to bypass it when the filter's pressure drop was higher than 17.2 kPa. Since the IPA produces a pressure rise of more than 41.3 kPa at the required flow rate of 0.76 l/min, and the pressure drop in the cooling-loop system was expected to be only 13.8 kPa, this additional pressure drop from a clogged filter was not anticipated to pose a problem in providing the required flow rate of Freon throughout the flight.

The exact reason for the clogging of the filter is still not known, because the cooling loop has not yet been disassembled. Even though the cooling loop was thoroughly cleaned and tested before the beginning of the life test, the clogging of this filter was surprising. Some speculate that a possible reason for the clogging was the presence of particles generated by the graphite within the Teflon flex line. The Teflon line was impregnated with graphite on its inside surface to prevent electrostatic discharge (ESD) caused by the flowing Freon from creating micro-holes in the Teflon that could lead to a leak within the cooling loop. A more definitive reasoning will be found after disassembly of the test loop. Since the flight filter has at least six times the capacity of the life test filter, engineers hope the flight filter will be less prone to clog. In addition, the flight filter's automatic bypass upon clogging provides further insurance.

High Current Draw of Stalled Pump

The flight-system primary pump was programmed to be on for the entire duration of the flight, with the secondary pump idle. The secondary was to be turned on automatically only if the primary failed. The main reason for leaving the secondary pump idle was to maximize its available life to serve as a full backup in case the primary failed. The power supply for the life test loop pump was connected to a relay preventing the pump from restarting automatically after a power outage; a manual switch for the relay would be used to restart the pump after a shutdown. This programming was done to prevent an unattended turn-on of the pump (and the possible consequent damage) during power surges typical during outages.

After almost one year of uninterrupted flawless operation of the life test loop, a power outage occurred, and the pump did not restart automatically, as designed. Following this outage, the pump was idle for about a month because of its unattended status. However, when an attempt was made to restart the pump manually, the 500-mA fuse was seen to be blown (normal current draw is 400 mA). Replacements of the fuse with those rated for as much as 1.5 A were unsuccessful in restarting the idle pump. Following these attempts, the pump was gently tapped twice and it restarted—the current draw was about 450 mA immediately after restarting and dropped down to its nominal value of about 400 mA in a few minutes.

During the period between this manual restart and the time when nominal steady-state performance was reached (a duration of less than 15 minutes), the current draw was also observed to momentarily rise to as much as 475 mA a few times. Simultaneous with these momentary peaks, an audible change in the pitch

of the pump would be heard when one could “observe” a flock of particles traveling through the loop via the pump.

Following this outage the pump was allowed to run for a few days and was deliberately turned off for two- to three-week periods to attempt repeating its failure to restart. Five such attempts to repeat this failure were unsuccessful. After these attempts, five more inadvertent power outages occurred, and in most instances the pump was off for about two or more weeks. In all cases the starting current required was higher than 500 mA. Also, in all cases except one, the pump started satisfactorily with a current draw larger than 500 mA, without any tapping of its body. In one instance, restarting the pump required a few gentle taps.

One theory that could explain all these effects is that the clogging of the filter followed by its bypass allowed the generated particles to collect within the loop without being removed from the flowing fluid. As long as the fluid was flowing, it would not allow particles to collect in one zone. However, upon stoppage of fluid flow after a power outage, the particles could settle in local “valleys” such as the gaps between the pump’s bearings. Since these bearings are hydrodynamically lubricated, the gaps are very tiny (6 to 18 μm wide), which implies that the particles could create enough friction to increase the starting current significantly.

Implications for the Flight System

The results of this long-term life test were used in the design and operation of the flight system. On the basis of recommendations made according to those results, the following steps were taken:

- The primary pump was maintained on and was not allowed to be turned off under any circumstance under the control of the mission operators.
- The secondary or backup pump, which was normally idle, was turned on for an hour once every two to four weeks to remove any settled particles, even though one would not expect any settling in zero gravity (during the life test power outages, the pump could always restart without any tapping as long as the idle period was less than two weeks, and two- to four-week frequency was practical for the mission).
- A filter much larger (6 \times) than that used for the long-term development-test loop was implemented for the flight system.
- The mechanical fittings (B-nuts) used for assembling the loop, which used soft-cone (aluminum) seals, were retorqued after a few days of the initial torquing, and epoxy was used on the exterior surfaces of the joints’ leak paths to provide as much insurance against leaks as possible.

The life test setup had operated continuously for 8000 hours before the actual launching of the MPF spacecraft in December 1996. The results from the operation of the life test are described in Ref. 12.72. The performance of the life test loop was continuously monitored and is shown in Fig. 12.34. This graph shows flow rate, pressure rise, and electric-power consumption of the pump. The test results showed no evidence of the corrosion after seven-month operation of the loop. The leak rate of the fluid from the system was minimal; it was much lower than the leak rate that was allowed in the flight system.

One lesson learned from the life test loop was that the backup pump needed to be turned on regularly to flush any particles that might settle in the pump bearings.

During the life test operation, the particles were observed to settle in the bearings and impeller area if the pump were stopped for an extended period of over four weeks. Based on this information, engineers decided to turn on the backup pump in the flight system for an hour once every month.

After the successful landing of the MPF on Mars in July 1997, the life test system was stopped. By this time the life test pump had continuously operated for more than 14,000 hours. The tubing and the fluid were investigated for corrosion and other particulate material. Of particular importance was the particulate that had clogged the filter during the life test.

The chemical analysis showed no evidence of corrosion in the aluminum tubing. The particulate in the fluid sample was found to consist of particles with sizes in the 1-to-40- μm range. The large particles were mostly silica, fibers, and some metallic particles. The smaller particles were mostly chromium, iron, and aluminum. The moisture levels were less than 5 ppm, whereas levels were about 17 ppm in samples taken at 5-month period. The organic residue found in the Refrigerant 11 was similar to the material used in the thread of the in-line filter. Most of the particles generated in the life test loop were found to be present because of the materials used in the life test setup. Except for the Teflon tubing and the chromium used in the pump, none of the other materials were used in the flight system.

The scanning electron microscopy done on the aluminum tubing indicated that the prominent mode of corrosion of the aluminum tubing was physical erosion by the chromium particles formed at the pump.

Performance of the Loop during Flight

The HRS performance was continuously monitored during the entire cruise to Mars. The HRS was first activated on the launchpad about two hours before launch. Both pumps were turned on, and the functioning of the system was verified by the current draw of the pumps. The temperature of the electronic equipment shelf and the radiator were also monitored to make sure the working fluid was flowing freely. About four hours after launch, the backup pump was turned off and only the primary pump remained on during the rest of the seven-month cruise. The backup pump was turned on once a month for an hour to ensure that no particulate accumulated in the idle pump.

The performance of the HRS during the initial periods was very close to the performance predicted and verified during the system-level thermal vacuum test. The equipment-shelf temperature was maintained at around $+5^{\circ}\text{C}$, whereas the radiator temperature was around -4°C . At these radiator temperatures, all the cooling fluid coming out of the equipment shelf was above 0°C , and the thermal control valve was completely open. All the fluid flowed through the radiator without any bypass. A temperature profile of the equipment shelf and the radiator for a one-hour duration on January 28, 1997, is shown in Fig. 12.35.

The radiator temperature was a function of the distance from the sun and the solar angle on the spacecraft. This temperature dropped as the spacecraft cruised away from Earth toward Mars. The temperature dropped from -4°C immediately after launch to below -12°C after 45 days into the cruise. At this time, the fluid

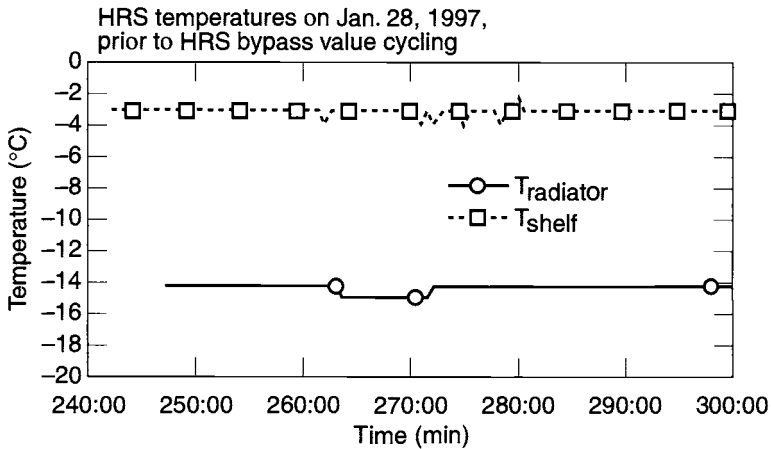


Fig. 12.35. HRS temperature during initial part of the cruise.

temperature coming out of the shelf was below 0°C . As this fluid entered the IPA, the wax-actuated thermal valve would open the bypass port, and part of the fluid would bypass the radiator. This bypass was designed to keep the electronics shelf above -7°C irrespective of the radiator temperature.

In Fig. 12.36, the temperatures of the equipment shelf and the radiator are shown for the day when the radiator bypass had just started. During this period, the shelf temperature was maintained between -4 and -2°C , while the radiator temperature varied between -16 and -14°C . The small fluctuations in the radiator and shelf temperatures were a result of the valve actuator's continuous attempts to adjust to the fluid temperature. This condition was observed and investigated during

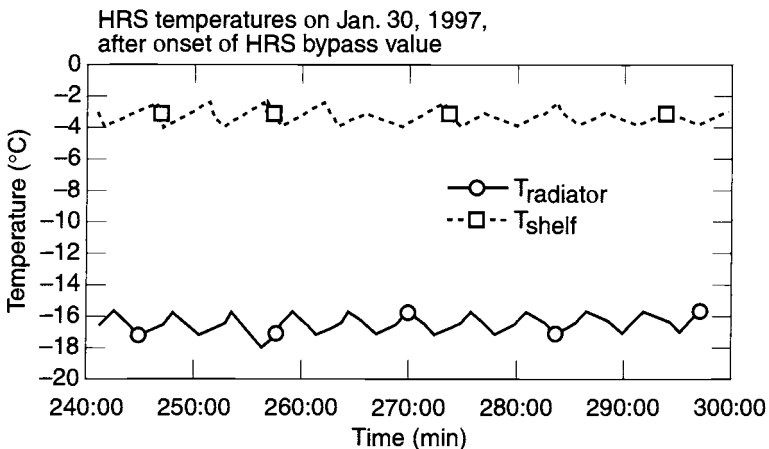


Fig. 12.36. HRS temperatures during latter part of the cruise.

the system thermal vacuum test. The fluctuation was attributed to an underdamped flow system and was considered harmless to the system.

While the spacecraft neared Mars, the radiator temperature gradually dropped to -70°C . However, the equipment shelf maintained its temperature at around -4°C . The radiator and the electronics-shelf temperatures during the complete mission are shown in Fig. 12.37.

The HRS was designed to vent all working fluid just prior to entering the Martian environment. About 90 minutes before the entry, the vent system was activated by the opening of a pyro valve that connects the high-pressure gas side of the accumulator to the liquid. The liquid was in turn vented to space via a nozzle, which is opened to space via another pyro valve.^{12.68} This event occurred on July 4, 1997, around 8 A.M. Pacific Standard Time. The spacecraft navigational data received by the ground controllers indicated that the nutation resulting from venting was less than two degrees and did not affect the spacecraft's course to the Martian landing site.

Mars Pathfinder PFL Summary

An active HRS consisting of a mechanically pumped single-phase liquid was designed and developed for the MPF mission. The unique requirements of the mission necessitated the use of the pumped-loop system for the thermal control of the spacecraft during its cruise to Mars. Because this was the first time that such a system was designed and flown, several new technologies were developed to make the loop successful, including the use of Refrigerant 11 (Freon-11) as a cooling fluid and a wax-actuated thermal control valve to bypass the flow. The Refrigerant 11 system allows the operation of the system at temperatures as low as -110°C .

MPF was the first U.S. deep-space mission to use a mechanically pumped cooling loop, and its successful flight demonstration showed that an active cooling system can be reliably used in deep-space missions. The data from the life test pump, combined with the flight data, show that the mechanical pumps can be reliably operated

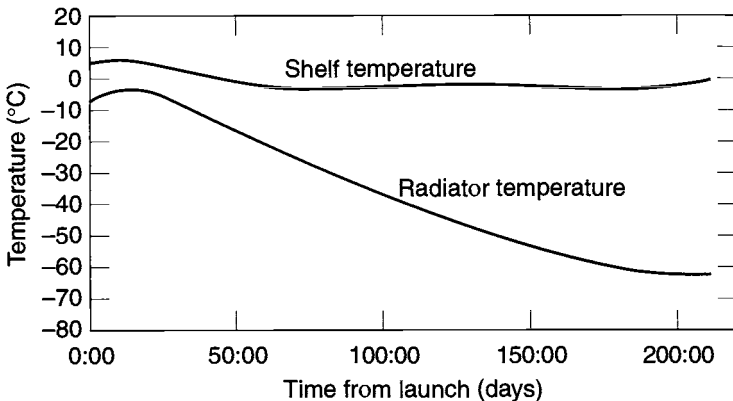


Fig. 12.37. Radiator and electronics-shelf temperatures during the entire cruise to Mars.

for missions lasting more than two years. The flexibility provided by the mechanically pumped cooling loop systems in the design, integration, test, and flight operation of spacecraft makes this cooling system ideal not only for faster, better, and cheaper missions but also for other missions.

References

Fluid-Flow Concepts and Basic Equations

12.1. W. M. Kays and M. E. Crawford, *Convective Heat and Mass Transfer*, 2nd ed. (McGraw-Hill, New York, 1972).

12.2. B. S. Petukhov, "Heat Transfer and Friction in Turbulent Pipe Flow with Variable Physical Properties," in *Advances in Heat Transfer*, Vol. 6, T. F. Irvine and J. P. Hartnett, eds. (Academic Press, New York, 1970), pp. 504–564.

12.3. M. N. Ozisik, *Heat Transfer—A Basic Approach* (McGraw-Hill Book Company, New York, 1985).

12.4. L. F. Moody, "Friction Factors for Pipe Flow," *Trans. Am. Soc. Mech. Eng.* **66**, 671–684 (1944).

12.5. "Flow of Fluids through Valves, Fittings, and Pipe," Crane Company, New York, N.Y., Technical Paper No. 410 (1982).

12.6. R. W. Fox and A. T. McDonald, *Introduction to Fluid Mechanics*, 3rd ed. (John Wiley & Sons, Inc., New York, 1985).

12.7. P. K. Swamee and A. K. Jain, "Explicit Equations for Pipe-Flow Problems," *Proceedings of the ASCE, Journal of the Hydraulics Division* **102**, HY 5, 657–664 (1976).

Forced Convection in Pipes and Tubes

12.8. J. P. Holman, *Heat Transfer*, 6th ed. (McGraw-Hill Book Company, New York, 1986).

12.9. M. N. Ozisik, *Heat Transfer—A Basic Approach* (McGraw-Hill Book Company, New York, 1985).

12.10. F. P. Incropera and D. P. DeWitt, *Fundamentals of Heat and Mass Transfer*, 2nd ed. (John Wiley & Son, Inc., New York, 1985).

12.11. S. R. Sellars, M. Tribus, and J. S. Klein, "Heat Transfer to Laminar Flow in a Round Tube or Flat Plate—The Graetz Problem Extended," *Trans. Am. Soc. Mech. Eng.* **78**, 441–448 (1956).

12.12. R. K. Shah and A. L. London, *Laminar Flow: Forced Convection in Ducts* (Academic Press, New York, 1978).

12.13. R. W. Allen and E. R. G. Eckert, "Friction and Heat-Transfer Measurements to Turbulent Pipe Flow of Water ($Pr=7$ and 8) at Uniform Wall Heat Flux," *Journal of Heat Transfer* **86**, 301–310 (1964).

12.14. A. P. Colburn, "A Method of Correlating Forced Convection Heat Transfer Data and a Comparison with Fluid Friction," *AICHe J.* **29**, 174 (1933).

12.15. F. W. Dittus and L. M. K. Boelter, *University of California (Berkeley) Publications in Engineering* **2**, 443 (1930).

- 12.16. J. P. Hartnett, "Experimental Determination of the Thermal Entrance Length for the Flow of Water and of Oil in Circular Pipes," *Trans. Am. Soc. Mech. Eng.* **77**, 1211 (1955).
- 12.17. R. H. Norris and D. D. Streid, "Laminar-Flow Heat-Transfer Coefficient for Ducts," *Trans. Am. Soc. Mech. Eng.* **62**, 525–533 (1940).
- 12.18. W. Nusselt, "Der Wärmeaustausch zwischen Wand und Wasser im Rohr," *Forsch. Geb. Ingenieurwes.*, **2**, pp. 309 (1931).
- 12.19. B. S. Petukhov, "Heat Transfer and Friction in Turbulent Pipe Flow with Variable Physical Properties," in J. P. Hartnett and T. F. Irvine, (eds.), *Advances in Heat Transfer*, Vol. 6 (Academic Press, Inc., New York, 1970), pp. 504–564.
- 12.20. E. N. Sieder and C. E. Tate, "Heat Transfer and Pressure Drop of Liquids in Tubes," *Industrial and Engineering Chemistry* **28**, 1429 (1936).

System Hardware

- 12.21. "Spacecraft Thermal Control Design Data," Vol. 2, Section Q, European Space Agency, (1981).
- 12.22. R. W. Fox and A. T. McDonald, *Introduction to Fluid Mechanics*, 3rd ed. (John Wiley & Sons, Inc., New York, 1985).
- 12.23. N. H. Afgan and E. U. Schlunder, *Heat Exchangers: Design and Theory* (McGraw-Hill, New York, 1974).
- 12.24. R. A. Bowman, A. C. Mueller, and W. M. Nagle, "Mean Temperature Difference in Design," *Trans. Am. Soc. Mech. Eng.* **62**, 283–294 (1940).
- 12.25. D. H. Fax and R. R. Mills, Jr., "General Optimal Heat Exchanger Design," *Trans. Am. Soc. Mech. Eng.* **79**, 653–661 (1957).
- 12.26. A. P. Fraas and M. N. Ozisik, *Heat Exchanger Design* (John Wiley & Sons Inc., New York, 1965).
- 12.27. K. Gardner and J. Taborek, "Mean Temperature Difference: A Reappraisal," *AIChE J.* **23**, 770–786 (1977).
- 12.28. J. P. Gupta, *Working with Heat Exchangers* (Hemisphere Publishing Corporation, Washington, 1990).
- 12.29. G. F. Hewitt (ed.), *Hemisphere Handbook of Heat Exchanger Design* (Hemisphere Publishing Corporation, Washington, 1989).
- 12.30. Hydraulic Institute, *Hydraulic Institute Standards for Centrifugal, Rotary and Reciprocating Pumps*, latest edition, Cleveland, OH.
- 12.31. W. Hyrnisak, *Heat Exchangers* (Academic Press, New York, 1958).
- 12.32. S. Kakac, R. K. Shah, and A. E. Bergles (eds.), *Heat Exchangers: Thermal-Hydraulic Fundamentals and Design* (Hemisphere Publishing Corporation, Washington, 1982).
- 12.33. W. M. Kays and A. L. London, *Compact Heat Exchangers*, 2nd ed. (McGraw-Hill Book Company, New York, 1964).
- 12.34. D. Q. Kern, *Process Heat Transfer* (McGraw-Hill Book Company, New York, 1950).
- 12.35. J. H. Lienhard, *A Heat Transfer Textbook* (Prentice-Hall Inc., New Jersey, 1981).

470 Pumped Fluid Loops

12.36. A.V. London, "Factors in the Selection of Pumps for Process and Chemical Duties," *Pumps-Pompes-Pumpen*, No. 88, pp. 25–31, 1974.

12.37. B. Nekrasov, *Hydraulic for Aeronautical Engineers*, translated from the Russian by V. Talmy, 1st ed. (MIR Publishers, Moscow, 1969) Chapter VI, pp. 80-87, Chapter XII, pp. 182–221.

12.38. D. R. Pitts and L. E. Sissom, *Heat Transfer, Schaum's Outline Series* (McGraw-Hill Book Company, New York, 1977).

12.39. F. Pollak and C. O. Cruger, "Comparison of Applications and Characteristic of Positive Displacement and Centrifugal Pumps," *Pumps-Pompes-Pumpen*, No. 96, pp. 400–407, 1974.

12.40. E. U. Schlunder (ed.), *Heat Exchanger Design Handbook* (Hemisphere Publishing Corporation, Washington, 1983).

12.41. G. Scobie, "Select the Pump that Meets Your Needs," *Chart. Mech. Eng.* **21** (51), 59–63 (1974).

12.42. G. S. Settles, J. T. Hamick, W. J. Barr, M. Summerfield, and M. Gunn, "Energy-Efficient Pumps Utilization," *J. Energy* **1** (1), 65–72 (1977).

12.43. R. K. Shah, A. D. Kraus, and D. Metzger (eds.), *Compact Heat Exchangers—A Festschrift for A. L. London* (Hemisphere Publishing Corporation, Washington, 1990).

12.44. K. P. Singh and A. I. Soler, *Mechanical Design of Heat Exchangers and Pressure Vessel Components* (Arcturus Publishing, Inc., Cherry Hill, NJ, 1984).

12.45. Standards of the Tubular Exchanger Manufacturers Association, Tubular Exchanger Manufacturers Association, New York (latest edition).

12.46. J. Taborek, "Evolution of Heat Exchanger Design Techniques," *Heat Transfer Engineering* **1**, 15–29 (1979).

12.47. G. Walker, *Industrial Heat Exchangers—A Basic Guide*, 2nd ed. (Hemisphere Publishing Corporation, Washington, 1990).

Working Fluids

12.48. *ASHRAE Handbook—Fundamentals* (American Society of Heating, Refrigerating and Air-Conditioning Engineers, Inc., Atlanta, latest edition).

12.49. R. C. Downing, "Refrigerant Equations," ASHRAE Paper 2313, Transaction of the American Society of Heating, Refrigerating and Air-Conditioning Engineers, 80, Part II, pp. 158 (1974).

12.50. E.I. DuPont de Nemours & Co., Bulletin T-11 (1972).

12.51. E. I. DuPont de Nemours & Co., Bulletin T-22 (1972).

12.52. E. I. DuPont de Nemours & Co., Bulletin T-502 (1969).

12.53. E. I. DuPont de Nemours & Co., Bulletin T-503 (1968).

12.54. L. Haar and J. S. Gallagher, "Thermodynamic Properties of Ammonia," *J. Phys. Chem. Ref. Data* **7**, 635–792 (1978).

12.55. J. J. Martin, "Thermodynamic Properties of Dichlorotetrafluoromethane," *Journal of Chemical and Engineering Data* **5**, 334–336 (1960).

12.56. J. J. Martin, "Thermodynamic Properties of Perfluorocyclobutane," *Journal of Chemical and Engineering Data* **7**, 68–72 (1962).

12.57. "Spacecraft Thermal Control Design Data," Vol. 2, Section Q, European Space Agency, (1981).

12.58. *Thermodynamic Properties of Refrigerants* (American Society of Heating, Refrigerating and Air-Conditioning Engineers, Atlanta, 1969).

12.59. N. B. Vargaftik, *Tables of the Thermophysical Properties of Liquids and Gases*, 2nd ed. (Hemisphere Publishing Co., Washington, 1975).

Analysis of a Fluid Loop

12.60. "Spacecraft Thermal Control Design Data," Vol. 2, Section Q, European Space Agency, (1981).

Computer Software for System Analysis

12.61. "RETRAN 02—A Program for Transient Thermal Hydraulic Analysis of Complex Fluid Flow Systems," Vol. 1: Theory and Numerics (Ref. 2), EPRI NP 1850 CCMA (1984).

12.62. T. M. Porsching, J. H. Murphy, and J. Redfield, "Stable Numerical Integration of Conservation Equations for Hydraulic Networks," *Nuclear Science and Engineering* **43**, 218–225 (1971).

12.63. "SINDA/FLUINT: Systems Improved Numerical Differencing Analyzer and Fluid Integrator," Cullimore and Ring Technologies, Inc. (1996).

12.64. "SINDA '85/FLUINT—Systems Improved Numerical Differencing Analyzer and Fluid Integrator," User's Manual, Version 2.3, Martin Marietta Denver Aerospace, Denver, CO (1990).

12.65. J. R. Turner, T. J. Swift, T. M. Andrews, and A. Lebru, "ESATAN FHTS—A Piped Fluid Network Capacity," *Proceedings of the 3rd European Symposium on Space Thermal Control and Life Support Systems, Noordwijk, The Netherlands, 3–6 Oct. 1988* (ESA SP-283, December 1988).

12.66. "SINDA/1987/ANSI Code," User's Manual, The Aerospace Corporation, El Segundo, CA (1990).

PFL Application

12.67. J. Lyra and K. Novak, "The Mars Pathfinder System Level Solar Thermal Vacuum Test," Paper No. AIAA-97-2454, *32nd Thermophysics Conference* (Atlanta, 23–25 June 1997).

12.68. P. Bhandari, G. Birur, and M. Gram, "Mechanical Pumped Cooling Loop for Spacecraft Thermal Control," Paper No. 961488, *26th International Conference on Environmental Systems* (Monterey, CA, 8–11 July 1996).

12.69. G. Birur, P. Bhandari, M. Gram, and J. Durkee, "Integrated Pump Assembly—An Active Cooling System for Mars Pathfinder Thermal Control," Paper No. 961489, *26th International Conference on Environmental Systems* (Monterey, CA, 8–11 July 1996).

12.70. G. Birur and P. Bhandari, "Mars Pathfinder Active Thermal Control System: Ground and Flight Performance of a Mechanically Pumped Loop," Paper No. AIAA-97-2469, *32nd Thermophysics Conference* (Atlanta, 23–25 June 1997).

12.71. G. Birur and P. Bhandari, "Mars Pathfinder Active Heat Rejection System: Successful Flight Demonstration of a Mechanically Pumped Cooling Loop," SAE Paper Num-

472 Pumped Fluid Loops

ber 981684, *28th International Conference on Environmental Systems* (Danvers, MA, 13–16 July 1998).

12.72. P. Bhandari and G. Birur, “Long Term Life Testing of a Mechanically Pumped Loop for Spacecraft Thermal Control,” Paper No. AIAA-97-2470, *32nd Thermophysics Conference* (Atlanta, 23–25 June 1997).